National Technical University of Athens
School of Civil Engineering
Department of Structural Engineering

BRIDGES SEISMIC ISOLATION USING CNT/POLYMER BEARINGS.

Postgraduate Thesis
By: Mohamed Attia

Under the supervision of:
Prof. Vissarion Papadopoulos

Submitted in partial fulfillment of the requirements
For the degree of Master of Science in Structural Engineering

ATHENS - JUNE 2021

ABSTRACT

Unfortunately, the structural health of bridges is continuously deteriorated over time due to the multiple-hazards like (earthquakes, winds, floods, traffic overload and accidents). These hazard events can be divided into 1) routine events and 2) extreme events. Routine events include overloaded truck, while extreme events include Hurricanes and earthquakes, and both of these events should be taken under consideration during the design in addition to the normal requirements. The main goal of this dissertation is to provide a method for bridges seismic isolation by using bearings from carbon nanotube (CNT) reinforced polymers. Carbon nanotube (CNT) reinforced polymers is such a prime example, where CNTs are used as inclusions to greatly enhance the mechanical properties of the parent material. Carbon nanotubes (CNTs) inspired many researchers and scientists in many applications according to its mechanical properties like the stiffness and damping, and thus CNT/polymer bearings are used as structural components for seismic isolation.

The dissertation has been divided into two parts: loading and assessment. A simulation-based and time history analysis methods are used to calculate the seismic load. The assessment part focuses on investigating the bridge safety by evaluating the super-structure to sub-structure connection against the seismic load, calculating the time period of each structure and checking the bending moment at the base of bridge piers.

Keywords: Hazard, Hurricane, Earthquake, Bridge, Damage.

Acknowledgment

First, I would like to thank Allah for the many blessings. I want to also thank my supervisor, Prof. *Vissarion Papadopoulos*, for being a source of support, advice, encouragement, and knowledge. I appreciate all his contributions of time, ideas, and stimulation. I would like to thank Dr. *Yiannis Kalogeris* for his support and help all the time.

I would like to thank Prof. *Michalis Fragiadakis* and *Maria Nerantzaki* for being on my committee, and for their helpful comments, instructive guidance for the duration of the dissertation review, and their insightful questions during the defense.

I would also like to thank my great professors, Prof. *Michael Kotsovos*, Prof. *Koumousis* and Prof. *Spiliopoulos*, for their support and help during all my study period at National technical university of Athens.

Lastly, I would like to thank my family for all their love and encouragement, in particular, my parents. And finally, I want to thank my best friends and another family, Ioana Damian, Marco Di Lascio, Giorgio Passos, Andrea Tappe, Marcel Honda and Adel Mohamed, who always encouraged me. Thank you all!

Contents

List of figures

Chapter 1 INTRODUCTION

The need for advanced high-performance materials in the industry led to the development of numerous innovative materials over the years, designed to possess application-specific properties. Carbon nanotube (CNT) reinforced polymers is such a prime example, where CNTs are used as inclusions to greatly enhance the mechanical properties of the parent material. So far, characterization of these materials mostly relied on extensive experimental efforts, which are both costly and time-consuming. In this regard, a promising approach towards replacing the experimental procedure is given by simulation-based material design that could drastically reduce the time and cost required for the characterization of CNT-reinforced polymers.

For the first part of the thesis, it focuses on the multiscale analysis for carbon nanotubes reinforced polymers based on a combination of hierarchical and semi-concurrent (FE^2) approaches as bridges between the multiple length scales, from atomic to micro to macro.

Carbon nanotubes (CNTs) inspired many scientists and researchers for wide range of electronics, optical, electromechanical and other applications and thus for the second part, CNT/polymer bearings with different weight fractions as structural components for seismic isolation were simulated using ABAQUS and used in the connection between a bridge superstructure and substructure as a solution for the catastrophic failure in this connection during the earthquakes event. Finally, trying to check the bridge health and evaluate the effect of these types of bearings.

Chapter 2 MULISCALE MODELING OF CARBON NANOTUBES

2.1 Introduction

The demand for more advanced material than the common ones led to a new generation of composite materials. Carbon nanotubes (CNTs) reinforced polymers is an important example of these composite materials, which consists of carbon nanotubes embedded into polymer matrix. Carbon nanotubes (CNTs) inspired many scientists and researchers for wide range of electronics, optical, electromechanical and other applications [1],[2]. Carbon nanotube can be considered as a sheet of graphite rolled in a tube and the properties of this tube depend on many factors like the atomics arrangement, the diameter and the length of the tubes, and the morphology. These rolled tubes molecular structure provide high stiffness and tensile strength which was proved also by experimental measurements [3], and therefore, reinforcing polymer matrix with CNTs can significantly improve the mechanical properties of the composite [4].

Considerable number of laboratory experiments have been done in order to determine the properties of these composite materials, which caused a great waste of time and costs due to trial-and-error loops [5],[6],[7],[8]. From here, the need for computational material design methods that can accurately predict the properties of CNT-reinforced polymers and thus replace these laboratory experiments to reduce time and cost. Multi scale simulation is used to model the material in different stages (atomic-micro- macro) to define the behavior of the material accurately and many multi scale finite methods have been developed to reduce the complexity of

the physical behavior at the different scales and the uncertainties of the material parameters [9],[10].

2.2 Modeling of carbon nano tube (atomic scale)

The equivalent continuum modeling (ECM) approach [11] is the most widely-used methods in atomic computational approaches as it was proved that it can be more efficient for the numerical modeling of CNTs than other most used approaches like ab into calculations [12] and molecular dynamics (MD) simulation [13] which are still not efficient for long time span or large scale systems and can used only in atomic scale and femtosecond time scale. In addition, the equivalent continuum modeling can make a link between the molecular mechanics and continuum mechanics as it can transform the chemical bonds between atoms in molecular mechanism atoms to continuum model using finite element method [14].

2.2.1 Molecular structural mechanics

Among the equivalent continuum modeling (ECM) methods, the molecular structural mechanics (MSM) approach proposed in [15],[16] has a big attention due to its effectiveness and simplicity. In this approach, the bonding force and Van der Waals (Vdw) interaction between two atoms of CNTs are represented by an equivalent round beam and a non-linear rod element, respectively as shown in fig. 1.

The potential energy Vt for a covalent bond system can presented by the equation in [17],

$$Vt = \sum V_r + \sum V_\Theta + \sum V_\varphi + \sum V_\omega + \sum V_{vdw}, \quad (2\text{-}1)$$

where V_r is the bond-stretching energy, V_Θ is the bond-angle variation energy, V_φ is the dihedral-angle torsion energy, V_ω is the inversion energy and V_{vdw} is the Van der Waals interaction

energy fig.1. The inversion energy can be inconsiderable comparted to terms of energy so it can be neglected in the case of the axial properties of CNTs but not the radial [11], and CNTs are neutral so the electrostatic interaction can be also neglected. Thus, calculation the protentional energy can be just for the first three terms in (2-1) equation.

The first three terms can be calculated under consideration of small deformation through the simple expressions.

$$V_r = \frac{1}{2} K_r (r - r_0)^2 = \frac{1}{2} K_r (\Delta r)^2 , \qquad (2\text{-}2)$$

$$V_\Theta = \frac{1}{2} K_\Theta (\Theta - \Theta_0)^2 = \frac{1}{2} K_\Theta (\Delta\Theta)^2 , \quad (2\text{-}3)$$

$$V_\varphi = \frac{1}{2} K_\varphi (\varphi - \varphi_0)^2 = \frac{1}{2} K_\varphi (\Delta\varphi)^2 , \quad (2\text{-}4)$$

where K_r is the bond-stretching force constant, K_Θ is bond-angle variation force constant and K_φ is torsional-resistance force constant, while Δr is the bond-stretching variation, $\Delta\Theta$ is bond-angle variation and $\Delta\varphi$ is the bond twisting-angle variation.

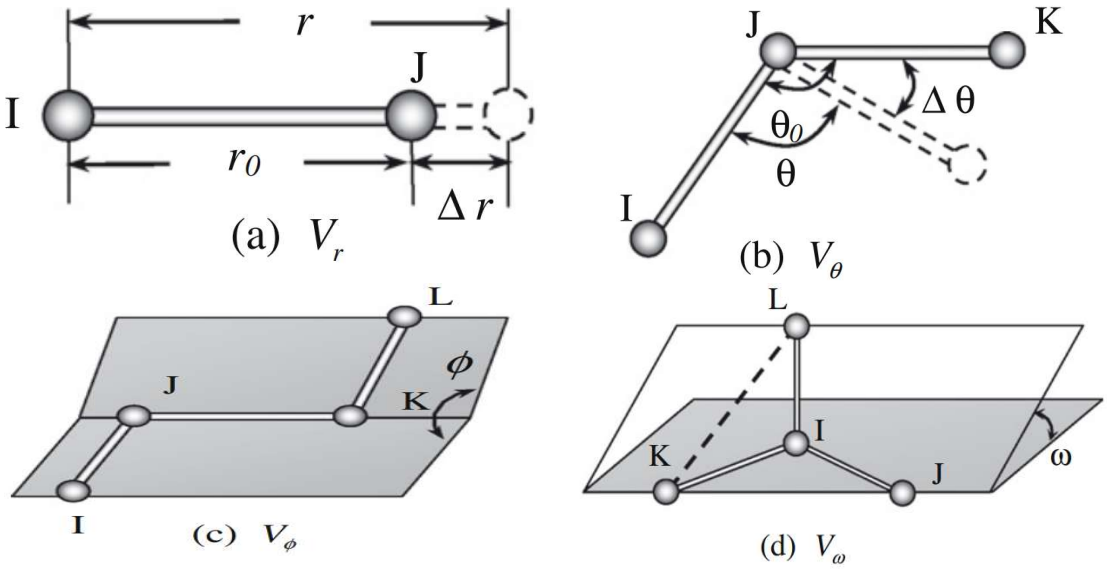

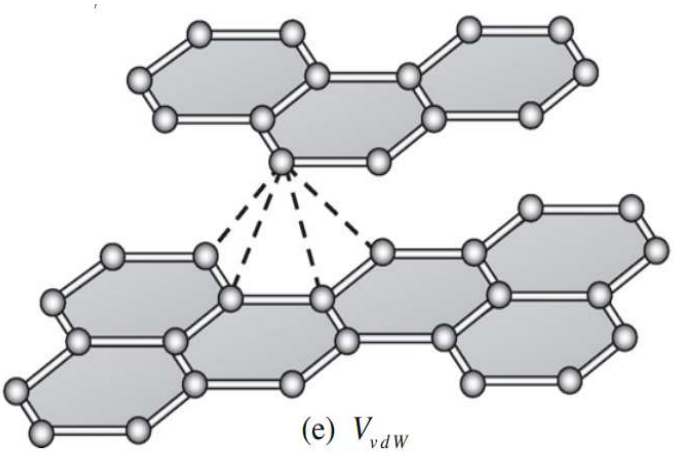

Figure 1 The potential energy for a covalent bond system

Going further, to determine the stiffness and other geometric parameters like young's modulus E,shear modulus G, length L, moment of interia I and polar moment of interia J, it is essential to get the relation between these parameters and the force constants in the molecular mechanism at first. The stiffness and these other parameters for the equivalent beam can be determined from the relation between the potential energy of the covalent bond according to atomic interaction and strain energy that was resulted by the structural deformation.

Assuming of uniform beam with a length L, Young's modulus E, and cross-section A, the strain energy of this unifrom beam due to axial normal force F_N in figure. 2a can be derived through,

$$U_{axial} = \int_0^L \frac{F_N^2}{EA} dl = \frac{1}{2} \frac{F_N^2 L}{EA} = \frac{1}{2} \frac{EA}{L} (\Delta L)^2, \quad (2\text{-}5)$$

Where ΔL is the axial dispalcement deformation. The strain energy of the uniform beam in case that it is subjected to bending moment M figuer.2b can be derived through,

$$U_M = \frac{1}{2} \int_0^L \frac{M^2}{EI} dl = \frac{M^2 L}{2EI} = \frac{1}{2} \frac{EI}{L} (\theta)^2, \quad (2\text{-}6)$$

where θ is the angle of rotation at the end of the beam due to the bending moment. In case that the beam is subjected to a pure torsian T figure.2c, strain energy can be derived through,

$$U_T = \frac{1}{2}\int_0^L \frac{T^2}{GJ}\,dl = \frac{T^2 L}{2GJ} = \frac{1}{2}\frac{GJ}{L}(\Delta\beta)^2, \quad (2\text{-}7)$$

Where Δβ is the relative rotation between the two ends of the beam.

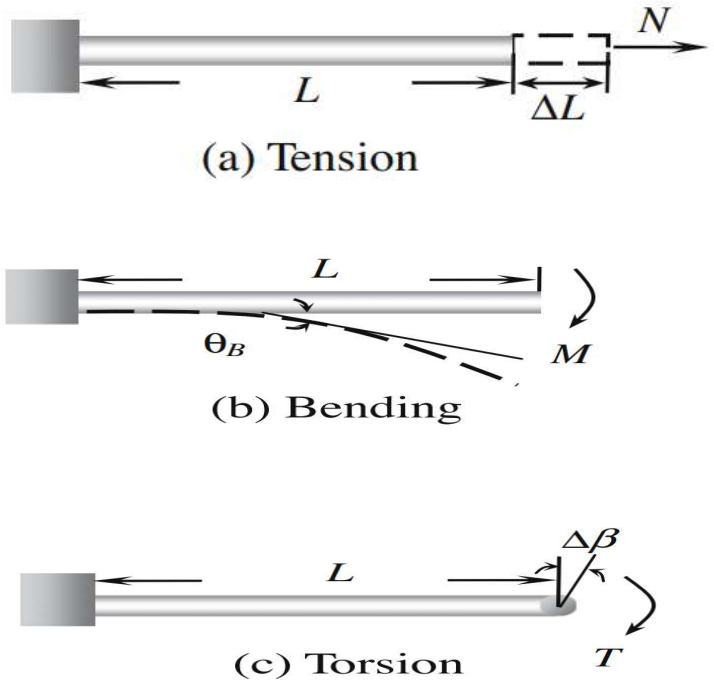

Figure 2 Deformation of a beam element

Regarding that Vr and U_{axial} are respresent the stretching energy, V_Θ and U_M represent the bending energy, and V_φ and UT represent the torsional energy. In addition, assuming Δr equal ΔL, Δθ and θ and Δφ equals Δβ. Thus, relating (2-2) to (2-5) and (2-4) to (2-7) yields the following relation between the structural mechanisms parameters and molecular mechanism force field constants,

$$K_r = \frac{EA}{l}, \quad K_\theta = \frac{EI}{L}, \quad K_\Phi = \frac{GJ}{L}, \quad (2\text{-}8)$$

K_r, K_θ and K_Φ are constants and L can be determined so E,G,A, I and J of the beam can be derived.

2.2.2 **Modified molecular structural mechanism**

Since assuming of the round beam and non-linear rod element which represent the bonding force and Van der Waals (Vdw) interaction between two atoms of CNTs in the original MSM, there is an equivalent bond bending rigidity in both the major and the minor principal centroidal axes of the cross section of the bond beam. The bending rigidity of that beam is derived from the bond-angle variation energy, and thus, this assumption may not be correct in theory as the beam bending rigidity in the minor principal centroidal axis should be closer to the weak inversion energy rather than the bond angle variation energy due to molecular mechanics. The inaccurate modeling of the sectional bending rigidity of the minor axis of the covalent bond will get a poor result for the radial stiffness properties of CNTs.

Initial derivation of the modified MSM model considered the graphite sheet as a frame structure. In figure. 3a, two of the hexagons in a graphite sheet, point O is the origin of the local Cartesian coordinate system for covalent beam OA. Assuming a single force F_x to the X axis at point B of beam OB, and therefore a moment M_z directed along the z axis. Since this moment M_z fully contribute to the bond angle variation energy between the bond OA and OB, the relation between the bending rigidity of the continuum pseudo-rectangular beam element around the major Z axis and the constant bond-angle variation force can be described by:

$$K_\theta = \frac{EI_z}{L}. \quad (2\text{-}9)$$

Moreover, another single force F_z parallel to the z axis is concentrated at point O and it cause a moment M_y around y axis. F_z force induce inversion energy V_ω between the atom O and

the three planes A, B and C, in Fig. 3b. M_y cause a contribution of one third of the inversion energy to the bending energy U_{My} of the covalent bond OA as described in:

$$U_{My} = \frac{1}{3} V_\omega = \frac{1}{6} K_\omega \theta_y^2 \text{ , (2-10)}$$

where K_ω is the inversion force constant and θ_y is the bending angle of beam OA along the Y axis. In addition, Integrating Eq. (2-6) with Eq. (2-10) result in:

$$K_\omega = \frac{3EI'_y}{L}. \text{ (2-11)}$$

By relating Eq. (2-9) with Eq. (2-11), this gives the relation of the moment of inertia around the minor I'_y and major I_z principal centroidal axes,

$$I'_y = \frac{K\omega}{3K\theta} I_z = .0058. I_z = k_1. I_z, \quad \text{(2-12)}$$

where K_θ is bond-angle variation energy.

It can be noticed from Eq. (2-12) that I'_y is much smaller than Iz, which means that the round beam in the original MSM model is clearly not conservative.

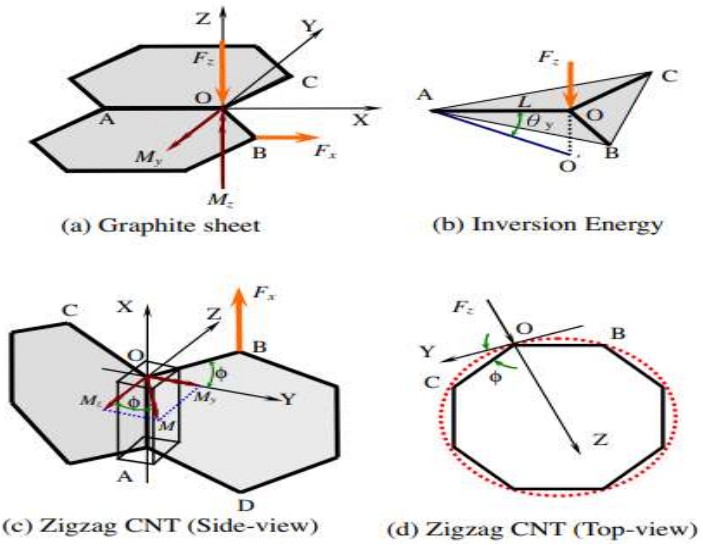

Figure 3 The moment of inertia of a covalent bond in the modified MSM model.

In case of SWCNT, a modification should be done for the previous derivation according to that it is a rolled-up graphene sheet rather than a plane one. Fig.3c shows two of the hexagons in a zigzag CNT, and Fig.3d is the top view of the CNT where is the red circular dots represent the ‘‘virtual” tube wall of the CNT, and the black segment lines are the actual tube wall. It can be noticed that the two hexagons in Fig.3c do not lie in a plane. Assuming that for OA beam, a local Cartesian coordinate system is also defined at point O, where the tangent line to the circular circumferential wall at point O is defined as the Y axis; the radial line passing through the center of the circular dot line, which is perpendicular to the tangent line, denotes the Z axis; and the axial direction of beam OA represents the X axis.

Considering angle φ between the tangent line at point O and the plane of the hexagons, the angle changes with the radius of CNTs. Moreover, the moment M on OA beam due to F_x acted on beam OB at point B in X direction. Moment M can be divided into two components,

My and Mz directed along the Y and Z axis, respectively, as shown in Fig.3c,

$$M_y = M \sin(\varphi) = \frac{E(I \sin\varphi)}{L}\,\theta = \frac{EI_y''}{L}\,\theta, \qquad (2\text{-}13a)$$

$$M_z = M \cos(\varphi) = \frac{E(I \cos\varphi)}{L}\,\theta = \frac{EI_z}{L}\,\theta, \qquad (2\text{-}13b)$$

I_y'' is the moment of inertial of beam OA directed around the Y axis due to the bond-angle variation energy V_θ. By comparing the two mentioned equations, relation can be written between I_y'' and I_z:

$$\frac{I_y''}{I_z} = \frac{(I \sin\varphi)}{(I\cos\varphi)} = \text{Tan } \varphi\ , \qquad (2\text{-}14)$$

And thus,

$$I_y'' = (\tan \varphi)\ I_z = K_2\, I_z. \qquad (2\text{-}15)$$

According to Eq. (2-6), the bending energy associated with these two moment components are

$$U_y = \frac{M_y^2 L}{2EI_y''},\ U_z = \frac{M_z^2 L}{2EI_Z}. \qquad (2\text{-}16)$$

The bond-angle variation energy V_θ between the covalent bond OA and OB is assumed to be equal to the sum of the above two terms

$$V_\theta = \frac{M_y^2 L}{2EI_y''} + \frac{M_z^2 L}{2EI_Z}. \qquad (2\text{-}17)$$

Thus, the following relation, similar to Eq. (2-9), can be obtained,

$$K_\theta = \frac{E(I_y'' + I_Z)}{L}. \qquad (2\text{-}18)$$

By Eq. (2-15) and (2-18) together, I_y'' can be obtained.

The inversion energy and bond-angle variation energy contribute to the energy of beam OA, the moment of inertia of this beam directed along the Y axis Iy can be calculated by the

$$I_y = I_y' + I_y''. \qquad (2\text{-}19)$$

The modified moment of inertia I_y and $I_{z\ can}$ be obtained. Fig. 4 displays the constants k1 and k2 varying with the radius of a zigzag SWCNT, and a larger radius would result in a decrease of k2. In addition, as the radius approaches to zero, k1 becomes far less than k2, indicating that the bending energy is dominated by the bond-angle variation energy V_θ. On the other hand, as the radius is larger than about 1.5 nm, k1 becomes larger than k2, implying that the bending energy V_θ and the inversion energy V_ω would both play an important part in the bending energy.

2.3 Modeling of carbon nano tube (microscopic scale)

For studying the material in different length scales, numerous multiscale methods have been proposed to account for the associating of different scales involved and the corresponding phenomena taking place at the interface of the CNT-RCs constituents. In general, multi scale approaches need to satisfy the conditions of conservation of total energy, mass, linear momentum and continuity of kinematic fields during her scaling of the solution. Among these methods, hierarchical or sequential or message passing multiscale methods are the most widely applied methodologies as a bridge between the atomic scale and microscopic scale [18].

2.3.1 Hierarchical multiscale methods

Hierarchical or sequential or message passing multiscale methods can be regarded under the type of coarse graining methods. Lower spatial scales are used as inputs to the next level scale in the simulation as the information is passing from the fine to the coarse scale. The basic assumption of multi-scale hierarchical methods is that the physics that control the process at different length scales can be easily separated and can be treated separately. The main principles at higher scales or coarse-grained scales can be defined by the higher-level boundaries or the input information from the lower length scales (the fine scales).

During transitioning to a higher scale, respect to time scale associated with higher level model is assumed and degrees of freedom associated with lower length scales have totally developed and can be considered frozen in time. The information which has been transited from the lower scale models will determine the parameters in higher spatial scale.

In coarse graining methods, the main idea is developing a functional form for the potential function controlling the coarse-grained system, and the functional form can be derived

by matching the protentional of the main force among interacting particles or the radial distribution functions or the average force at predetermined coarse-grained sites for the atomic scale.

Hierarchical multi scale methods have two major limitations. The first one is that the nature of dependence of physical laws governing different length scales must be known as the information received from the lower scale must be utilized in determining the parameters govern the process at coarse length scale, and thus the accuracy of coarse scale parameters depends of the accuracy of lower scale simulations. The second limitation, if the governing laws for different scales show high dependence on each other, one time exchange information from lower scale to higher scale will not be sufficient and it leads to the requirement of interactive approach.

Hierarchical methods are computationally less expensive. In the case of mechanical response of nano composites evaluation, transitioning between multi scales through physical quantities is well established, and this, hierarchical methods are the most common ways used in studying the mechanical response of nano composites.

2.4 **Modeling of carbon nano tube (macroscopic scale)**

The definition of the macroscopic response of materials that are heterogeneous and have a complex microstructure in the sense homogeneous, and has always been defined as a transition from micro to macro, is an important component of continuum micromechanics. In recent years, several numerical methods have been developed which discretize fine scales on the representative microstructure. These numerical methods can be used to get information on the mechanisms of fine scales and allow the analysis of nonlinear geometries of composite cells.

2.4.1 **Concurrent multiscale methods**

Concurrent multiscale methods are relatively new area of material computational simulation. The information changes simultaneously between different spatial scales and different levels. The modeling scheme does not require any assumptions about the physical phenomena under consideration. The process develops according to the constitutive laws of each length scale and the coupling among them, and inter-dependence is not required on prior information scale. In concurrent methods the total simulation is performed in one step. These methods require a good domain portioning strategy to provide suitable representation for each length scale in the model.

Ensuring a continuous seamless exchange of information between different spatial levels becomes very complex, in particular, if material systems, are different scales in modeling show poor dependence on each other, and thus, accurate handshake coupling is essential to facilitate seamless exchange of the information among regions representing the different spatial scales. However, the main challenge in concurrent methods is the dynamic tracking of region portioning boundary which is tie down to the choice of handshake method which is physically consistent and accurate while computationally less expensive.

2.4.2 **Homogenization scheme**

As mentioned before about trials and approaches for the transition from micro to macro, the paper [19] provided the outline of algorithms and represented matrix to describe the overall stresses and tangent moduli for microstructure of heterogenous material under small strains and related to linear displacement. The homogenization scheme can be applied to the microscopic

finite element model of a RVE of polymer matrix and a linear EBE which representing the CNT reinforcement inside the matrix, and according to it, for a given macroscopic strain $\bar{\varepsilon} = [\ \bar{\varepsilon}_{11}\ \bar{\varepsilon}_{22}\ 2\bar{\varepsilon}_{12}\ ]^T$ a displacement field u can be applied to the boundary of the RVE according to the relation: $u(x) = \bar{\varepsilon}\, x$ at $x \in \partial V$, (2-20)

where x denotes the position vector of a point on the boundary of the RVE and ∂V denotes the boundary of the RVE. The aforementioned relation constitutes the localization rule can be used to transition from the macroscopic to the microscopic level.

After the solution of the boundary value problem resulting from the application of the localization rule, the macroscopic stress $\bar{\sigma} = [\ \bar{\sigma}_{11}\ \bar{\sigma}_{22}\ \bar{\tau}_{12}\ ]^T$ can be calculated as the volume average of the microscopic stress σ according to the relation:

$$\bar{\sigma} = \frac{1}{\|V\|}\ \mathrm{sym}\ (\int_V \sigma\ dv), \quad (2\text{-}21)$$

where $\|V\|$ denotes the volume of the RVE. Eq. (2-20) is the homogenization rule, that is, the rule that yields the macroscopic state variables as a function of the microscopic stress state; in other words, the homogenization rule is used to transition from the microscopic level back to the macroscopic one. This transition from the microscopic to the macroscopic and vice versa is schematically depicted in Fig. 4.

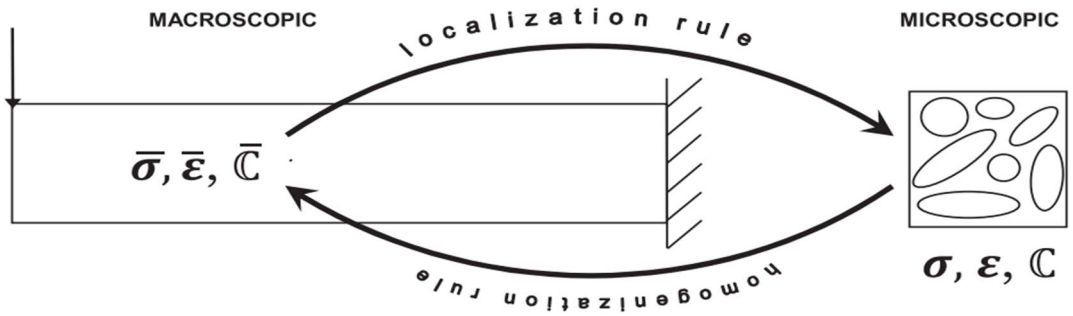

Figure 4 Overview of the solution scheme.

Finally, the macroscopic tangent modulus C can be calculated as the sensitivity of the macroscopic stress σ with respect to variations of the macroscopic strain ε according to the relation:

$$\bar{C} = \partial\varepsilon\ \overline{\sigma}\ .\ (2\text{-}22).$$

Chapter 3 THE IMPACT OF INTERFACIAL SHEAR STHEGTH AND WEIGHT FRACTION ON THE MACROCOPIC PERFORMANCE OF CARBON NANOTUBE COMPOSITES

3.1 Introduction

According to the small nanometer scale and the low density, the surface area to the mass ratio of carbon nanotubes CNTs regards as extremely large, and thus in a nanotube-polymeric composite structure, high damping can be achieved through the advantage of the interfacial friction between the nanotubes and the surrounding polymer resin [20], and it was proved that the Interfacial shear strength (ISS) and weight fraction (WF) can significantly affect the mechanical performance of carbon nanotube (CNT) reinforced composites.

In general, the value of ISS can be changed greatly with the treatment methods of the surface of CNTs, and thus, the ISS values for CNTs with untreated surface is low value as the interaction with polymer is mainly via van der waals forces [21] . But it is proved that functionalization process can result in strong covalent bonds between chain of polymers on the surface of CNTs and surrounding polymer.

Many researches have been done to identify the mechanism of stress transfer at the carbon nanotube-polymer interface, however, there is still a paucity of the scientific date which describe that interaction mechanism and it raises questions about the constitutive relations of interfacial shear stress. Pullout experiments of multi-walled CNTs in [22] showed that the pullout process is

more brittle rather than ductile for short embedded lengths and it means that the interface of CNT-matrix fails because of the spread of a crack along the interface. On the other hand, for larger lengths, it shows some friction interaction between the CNT and matrix after failure of the CNT-matrix interface. Going further to [23] as the simulation attempt for the pullout of multi wall CNTs from a polymer matrix using van der waals as a description for CNT-matrix interaction showed that the pullout process is ductile and it leads to the inconsistencies between the experiments and numerical simulation about the nature of the interaction between CNTs and other materials.

Many researches have been done with different multiscale methods to define the impact of ISS and weight fraction on the macroscopic performance of carbon nanotube composites and it will be showed next.

3.2 **Literature review**

In [24], a CNT/polymer cantilever beam was analyzed using a three-level multiscale technique. At the atomic level, a short CNT was modeled as a space frame structure, using the modified molecular structural mechanism (Mmsm), moving to microscopic level, a presentative volume element (RVE) consisting of a polymer matrix reinforced with a single horizontal CNT described at the previous level is analyzed using the finite element method and finally for the macroscopic level, a cantilever beam consisting of the material described by the RVE of the previous level is analyzed using the finite element method. The space frame structure was projected on an equivalent beam element (EBE) and sequential multiscale technique was applied for the transition from atomic to microscopic level. The microscopic linked to macroscopic level using the semi concurrent multiscale technique was applied and first order homogenization

scheme in conjunction with a FE^2 . the cantilever beam was loaded with a vertical load of a unit magnitude (in GN), scaled by a loading factor λ which is between 0.03 and -0.03.

A polymer matrix reinforced with straight, unidirectional CNTs was analyzed. The matrix and the CNTs were considered linearly elastic. The matrix was composed of polyether-ether-ketone (PEEK), elastic modulus E_m = 2.79 Gpa and Poisson's ratio equals 0.4. The nanotubes were single-walled, with a nominal outer diameter of 14 nm, and their chirality was type armchair (100,100). Several CNT weight fractions were considered, ranging from 0.1 to 2%, which were obtained by varying the matrix thickness. Bond slip model was used for modeling the CNT-PEEK interaction.

For the results, it was observed that it can be no stress transfer between the CNT and the polymer if ISS = 0 and on the other hand, full bond can be existed in case that ISS = ∞ as shown in fig. 5. Moving to fig. 6 which represent the relation between the damping ration ξ and ISS with various weight fraction and strain amplitude, it can be noticed that larger weight fraction yield larger damping ratio coefficients for smaller ISS values and the peak value for damping of each curve represent specific weight fraction is shifted to lower ISS values for larger weight fraction. The peak for each curve is related to the ISS values where the full slippage has done for the CNT as the strain applied is equal to strain amplitude, and thus, if there is no slippage for the CNT at the RVE's most strained state, the damping ratio is lower than the peak value. It can be noticed also that when the strains are increasing, the maximum value of damping for specific weight fraction does not change but just shifted to higher values for ISS.

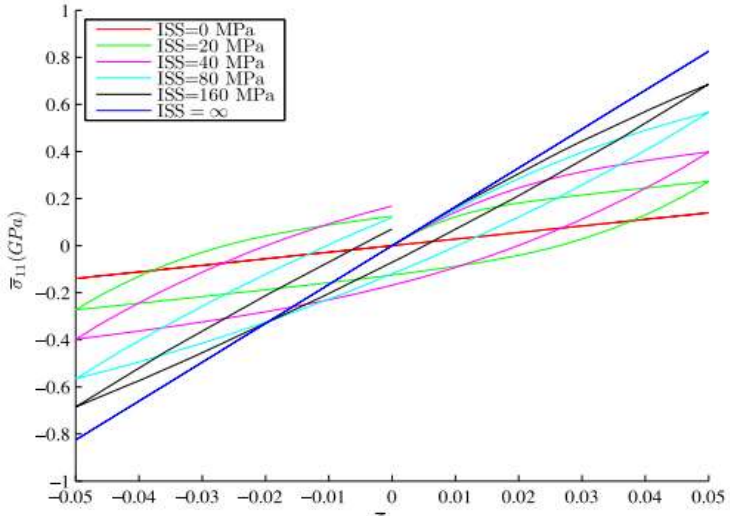

Figure 5 Variation of the homogenized stress σ_{11} with respect to the applied strain ε_{11} for weight fraction equal to 1% and strain amplitude equal to ε_{max} = 5%.

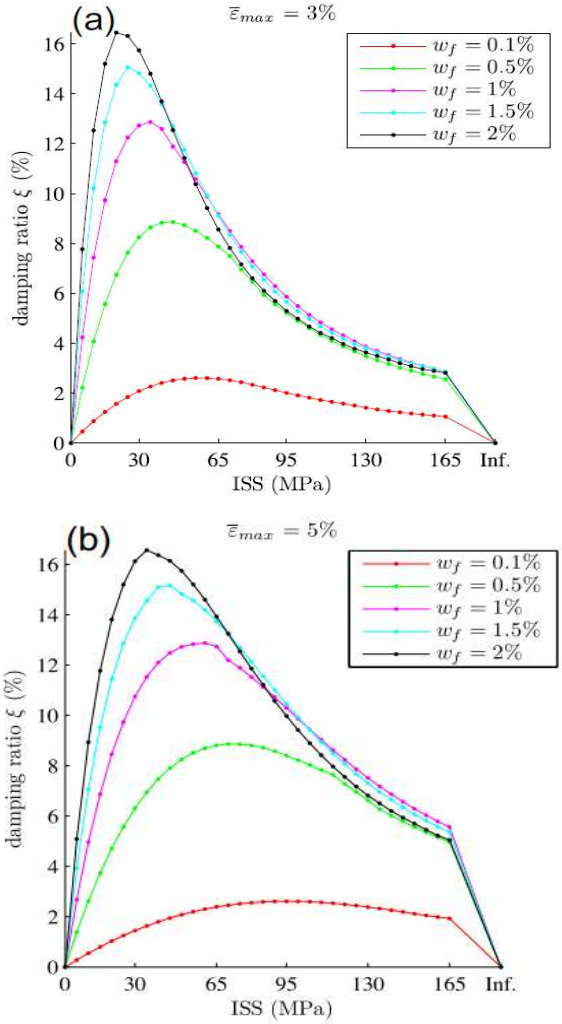

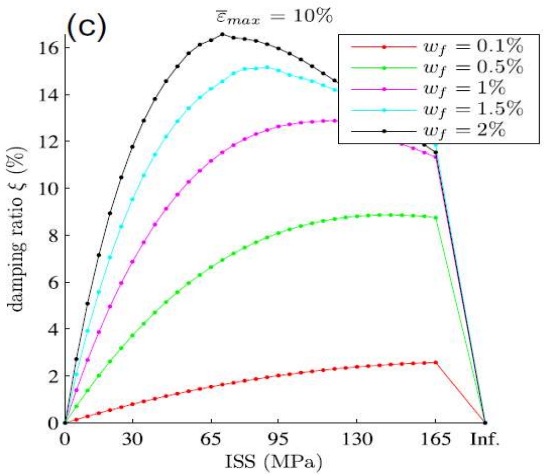

Figure 6 Variation of the damping ratio ξ with respect to ISS for various weight fractions and strain amplitude equal to (a) ε_{max} = 3%, (b) ε_{max} = 5% and (c)ε_{max} = 10%.

To investigate the impact of ISS and CNT weight fraction on the overall behavior of macroscopic structures Figure. 7 display the force–displacement curves of the structure for various ISS values and weight fractions equal to 0.5 and 1 % respectively, and it was observed the same in the microscopic case as higher ISS values lead to a stiffer structure for a certain weight fraction.

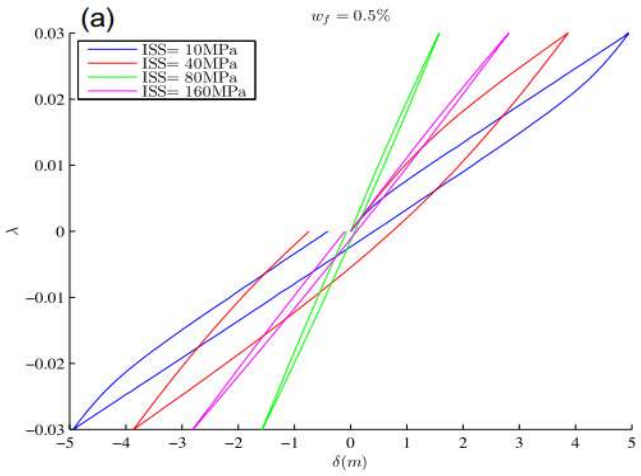

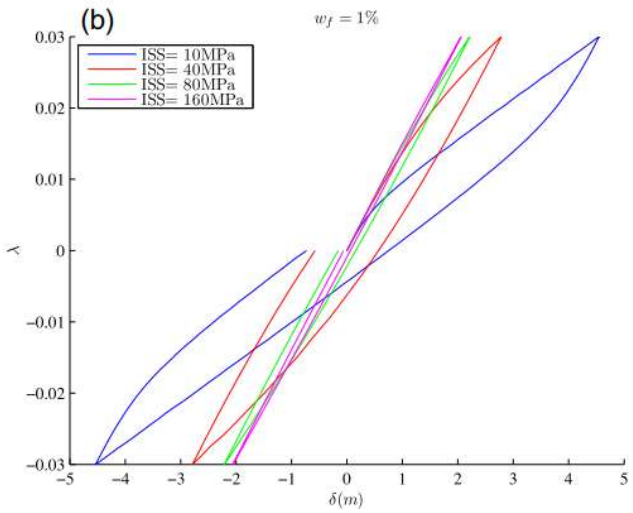

Figure 7 Force–displacement curves of the macroscopic model for two weight fractions (a):0.5% and (b):1%) and various values of ISS.

Moving to [14] for investigating the mechanical and damping properties of the carbon nanotubes reinforced composites CNT-RCs with the respect of various weight fractions from 0.1% to 2% and interfacial shear strength using multiscale analysis. At the atomic level, the lattice of CNTs was modeled using the modifies molecular structural mechanism MMSM approach as a space frame structure. The more details of the nanostructure in the MMSM approach leaded to various computational efforts, and thus the MMSM model was reduced to equivalent beam element EBE which was the basic at the micro scale and embedded to the polymer grids. Linear material properties were specified to the equivalent beam elements, and a Maxwell–Weichert material model was used for modeling the viscoelastic behavior of the polymer. The interfacial load transfer between the lateral surface of the CNTs and the surrounding matrix with the consideration of non-linear bond slip friction type.

Both the influence of straight and wavy CNT was considered and stochastic average properties were acquired by Monte Carlo simulations.

For the straight CNTs, multi wall CNTs were used with outer diameter of 14 nm corresponding to the outer CNT of chirality type armchair (100,100), the molecular modified structure mechanism space frame was reduced to linear equivalent beam element EBE with a wall thickness t = 0.34 nm and a pipe profile section. Young's moduli equal 1.051 Tpa and shear moduli equals 0.503 Tpa. Representative volume elements were subjected to monotonic and cyclic axial loading with 1 Hz frequency, and strain amplitude 5%.

It was observed that all the CNTs are strained less than 1% for the considered cases, and thus it was leaded to linear elastic assumption for the CNTs. Furthermore, the effect of the ISS on the damping and stiffness properties was observed for various values for the ISS from 5 to 80 MPa.

Figure.8 shows the stress and strain diagrams for the above-mentioned values of the ISS, with assuming an elastic behavior for the polymer and it is obvious that the stiffness and the energy dissipation capability of the CNT reinforced composite is increased with increasing ISS.

Moving to the wavy CNTs, the random CNT waviness has been considered by performing stochastic analysis. a number of random CNT geometries were generated and the corresponding

RVE FE models with Wf around 2% were analyzed in the context of a Monte Carlo simulation for cyclic loading and ISS = 40 MPa.

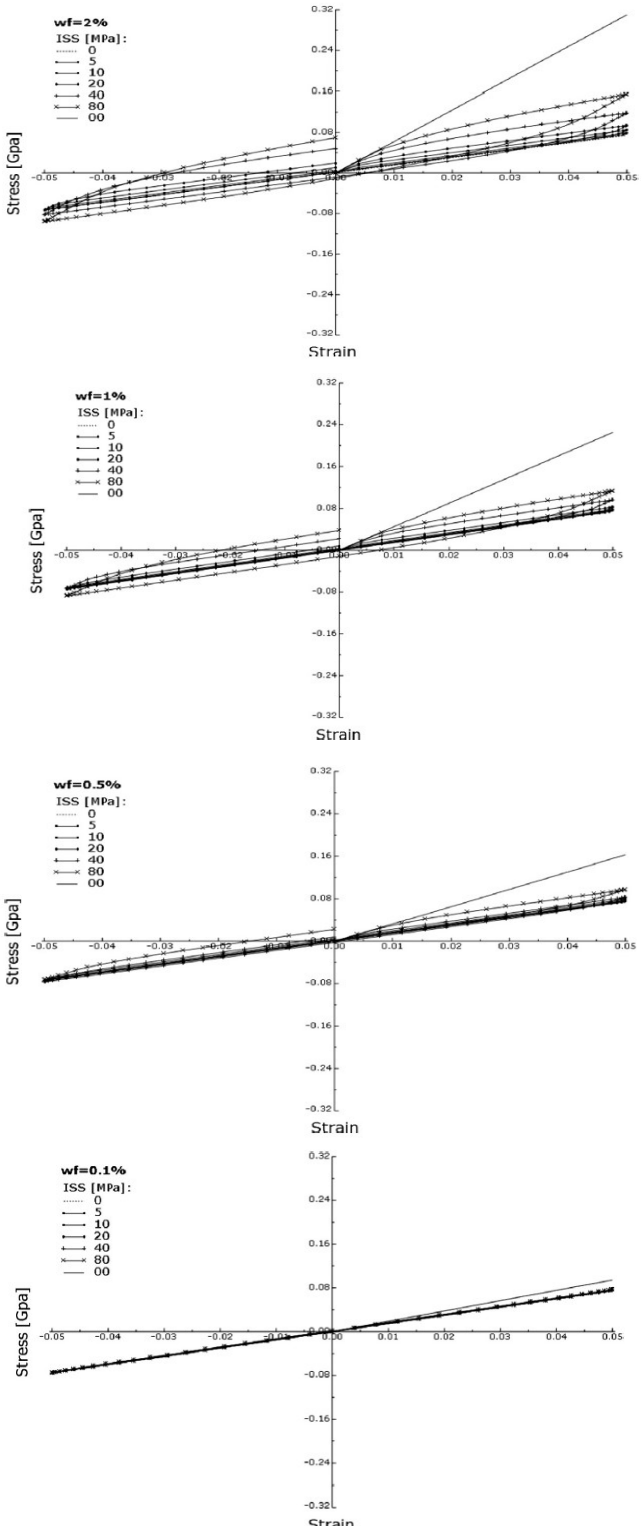

Figure 8 Stress–strain curves for CNT-RC RVEs considering linear elastic polymer, wf = 2,1,0.5,0.1 and ISS = 0,5,10,20,40,80,∞ MPa

To observe and compare between the straight and wavy CNTs, the average curve was estimated from the cloud of the computed stress–strain curves presented in fig. 9, and it was found that CNT length was the same in all RVE models, thus the observed differences in the stress–strain curves were according to exclusively attributed to CNT stochastic waviness. From these curves also observed that CNTs straightening is leading to improved damping properties of the CNT-RCs as the values of the loss factor were obtained in the case of the straight CNT equals 0.3744 and in case of wavy CNTs equals 0.3182.

Furthermore, in [25], a study to investigate the deflection of carbon nanotube (CNT) reinforced polymer composite beams. The effects of volume fraction of CNTs and the nanotube diameter were also considered on the beam deflection and comparisons were made with carbon fiber reinforced composites. The models were used in this study include straight CNTs aligned in one direction and randomly oriented.

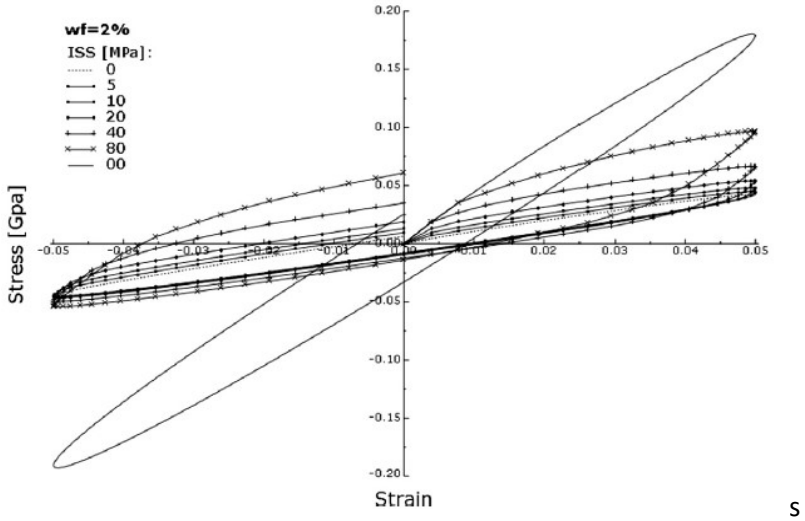

s

Figure 9 Comparison between average stress–strain curve of 50 RVEs with random wavy CNTs with the corresponding RVE with a straight CNT.

For the aligned nanotube reinforced laminate and the randomly oriented nanotubes, the diameters of the nanotubes are taken as 2A ˚ and it was observed that the deflection of the beam decreased clearly at low volume fraction of nanotubes, and thus the stiffness increased. Also, it was be noticed that lower nanotube diameters lead to lower deflection indicating higher stiffness.

Figure. 10 shows the relation between the decrease in maximum deflection and the increase in the volume fraction of nanotubes for five stacking in sequence where w0 is the maximum deflection of the unreinforced beam, and it is also clear that however the effect of the diameters of nanotubes on the deflection, it also depends on the stacking sequence. As also mentioned according to the results, the minimum deflection was obtained for the stacking sequence (0º/90º/0º/90º), the highest ones for sequence (90º/45º/-45º/0º).

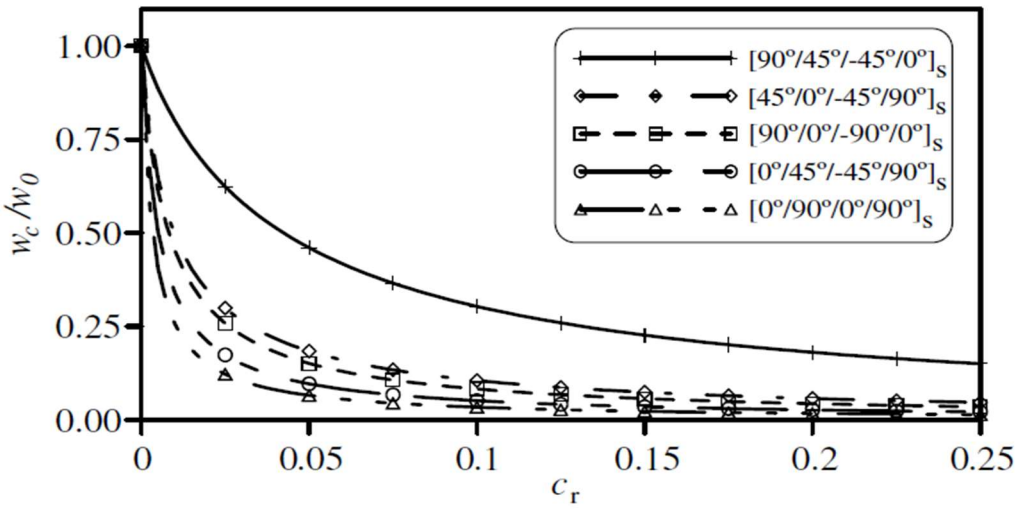

Figure 10 Curves of maximum deflection plotted against CNT volume fraction Cr for various stacking sequences

Chapter 4 BRIDGES SAFETY AGAINST EARTHQUAKE-HAZARD

4.1 Introduction

Multiple hazards (e.g., earthquake, wind gust, flood, vessel collision, traffic overload and accidents, and terrorist attacks, etc.) must be properly considered in the bridges design in addition to the normal functionality design requirements. Unfortunately, the structural health of bridges is continuously deteriorated over time with the increase of natural hazard events.

Many attempts have been done to investigate bridges safety against multi-hazard by obtaining load scenarios and evaluation of the performance based on these loads. Hazard events have been divided into routine events and extreme events. Each part of such events has been divided into loading part which aims to better understand the current loads, how it grows and resist if it is possible, and assessment part which is aiming to check bridges safety and suggest solutions to maintain the healthy case. Routine events can be presented by overloaded truck, while extreme events presented by Hurricanes and earthquakes.

4.2 Seismic design of bridges

4.2.1 Structural systems

In general, Bridges consist of many structural components (decks, piers, abutments and wing wall) as shown in figure. 11. In addition, there are many different structural systems and each structure system has its advantages and disadvantages. Simply supported spans structural

system as shown in figure. 12 can be perfect in the case of precast beams in addition to the advantage of differential settlements and tectonic displacements.

However, the disadvantages for this structural system can be presented in the presence of the large moments in the mid span and the exist of deck fall danger during the earthquakes. Moreover, this type of structure has no clear seismic response due to asynchronous movement of decks and the danger effect of the impact between adjacent decks.

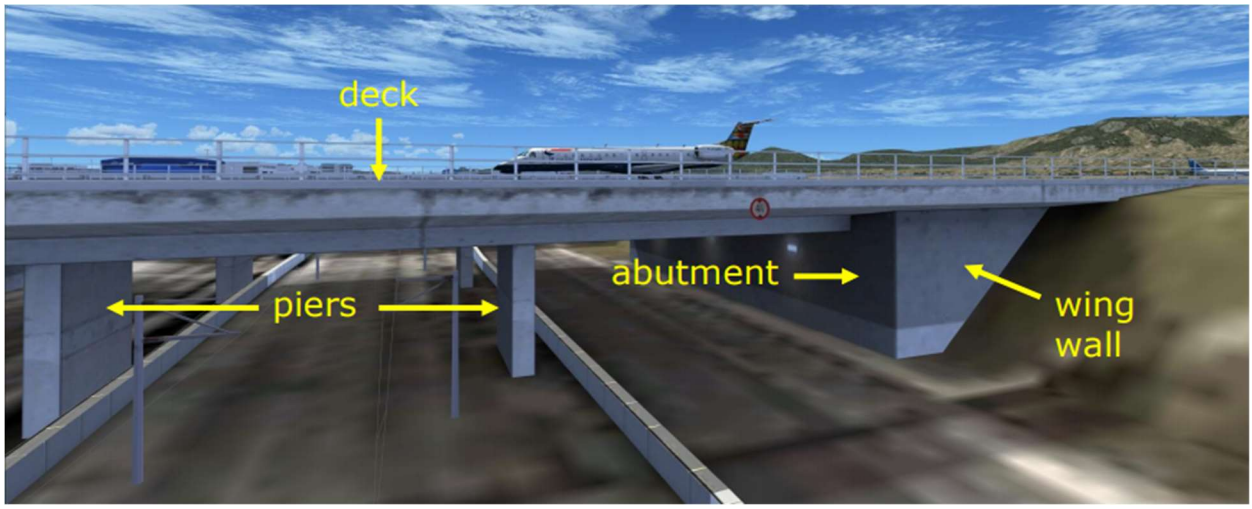

Figure 11 Structural components of bridges.

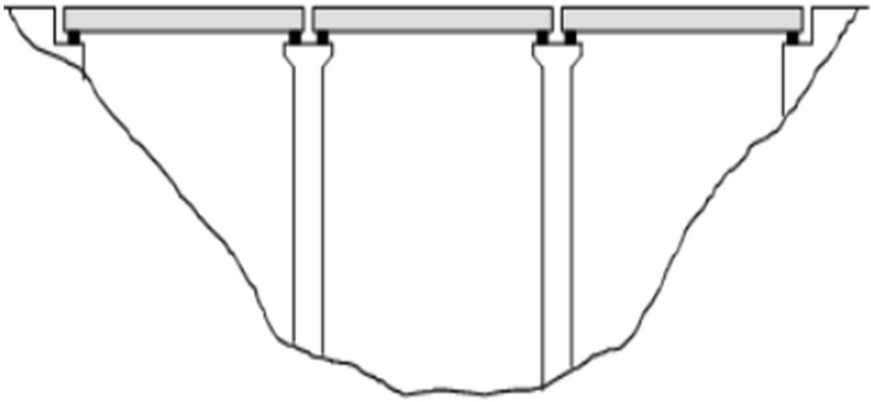

Figure 12 Simply supported spans structural system

While the continuous deck structural system as shown in figure. 13 can give a good distribution moment between supports and spans and good seismic behavior as all piers move similarly and, no danger of deck fall. In addition, the deck of the bridge in this case has a small thickness.

On the other hand, the system is not suitable for differential settlements and tectonic displacements.

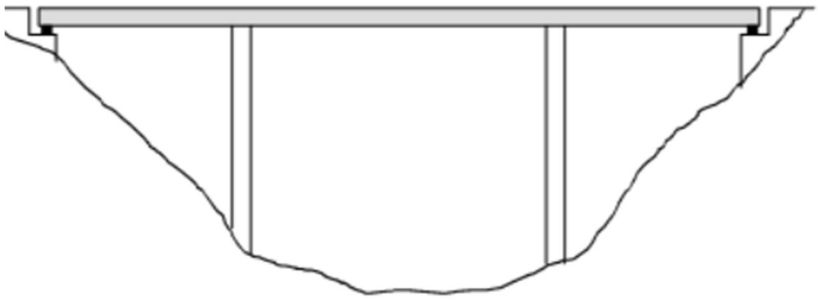

Figure 13 Continuous deck structural system

Moving to decks with Gerber beams structure as shown in figure. 14**,** it is clear that this structure can be the best balancing for moments between supports and beams but in the same time due to narrow supports, it can lead to serious danger of deck fall during the earthquakes. Therefore, special connection systems are required to reduce possibility of fall.

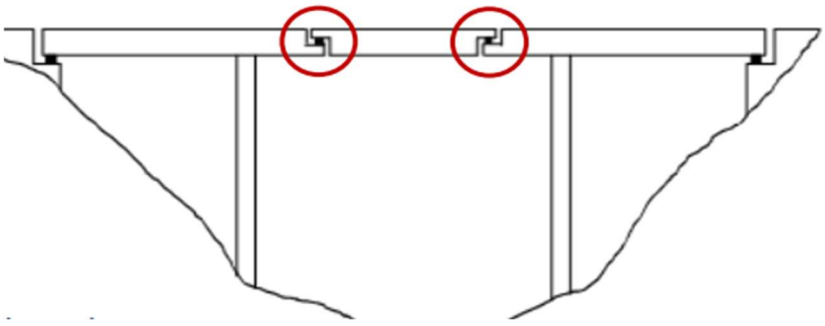

Figure 14 Decks with Gerber beams structural system

4.2.2 **Pier-to-deck connections**

As shown in figure. 15, there are two types of pier to deck connections. The first one is the monolithic connection which regards as stiff structure as there are just small displacements.

On the other hand, it can lead to develop of seismic moments on the deck in addition to thermal vibrations, shrinkage and creep which produce deformations on the piers.

For the second types of the connection is through bearings which divided into two systems: continuous deck and simply supported spans. For this connection can be regarded as seismic isolation system according to its flexibility, but the disadvantages of this connection can be presented in the larges seismic displacements which can lead to deck fall. In addition, piers in this can case behave like cantilever as larges moments can be produced on the base.

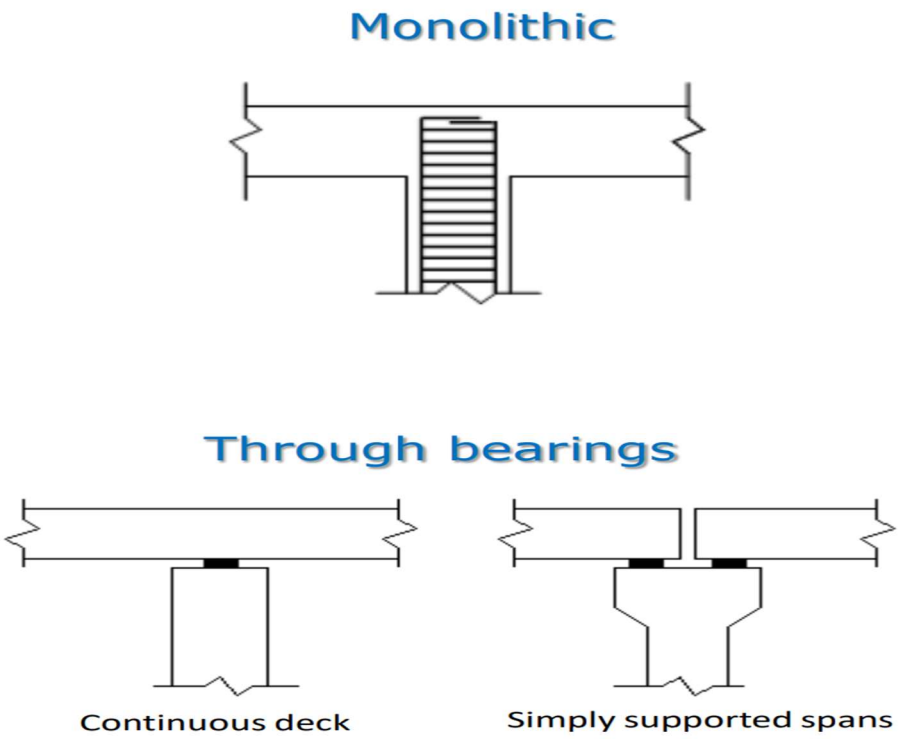

Figure 15 Piers to deck connections types

For the most common bearings types for the pier to deck connection, shown in figure. 16, can be presented in laminated elastomeric bearings which allow horizontal displacements and rotation, pot bearings which allow just rotations and sliding bearings which consist of elastomeric or pot bearing with sliding mechanism in one or both directions or it can be friction pendulum systems FPS which provide recentering at the end of seismic motions.

Figure 16 Common types of bearings

4.2.3 General principles of seismic design

There are many general principles of seismic design should be taken under consideration for bridges: first of all, bridges are simple structures from the structural point of view. However, they are also sensitive structures. In most cases, inelastic response of the piers is allowed and Plastic hinges are allowed only in the pier. On the other hand, the bridge deck has to remain within the elastic range. Flexural hinges need not necessarily form in all piers, but the optimum behavior is achieved if plastic hinges develop approximately simultaneously in as many piers as possible and the location of plastic hinges should be selected at point accessible for inspection

and repair as far as possible. Moreover, plastic hinges must not be formed in reinforced concrete sections where the normalized axial force is large.

4.2.4 Seismic action according to EC8-1 (2004)

In EC8-1 (2004) the seismic action is defined in terms of a single parameter, specifically the value of the reference peak ground acceleration on type A ground, denoted as a_{gR}. The reference peak ground acceleration a_{gR} for use in the seismic design may be derived from zonation maps provided in the National Annex of each Country. The reference peak ground acceleration corresponds to the reference return period $T_{RP,R}$ = 475 years of the seismic action for the no-collapse requirement. Return period $T_{RP,R}$ = 475 years is equivalent to probability of exceedance PR = 10% (reference probability of exceedance) in TL,R = 50 years (reference life of structures). For return periods $TRP \neq TRP,R$, the design ground acceleration on type A ground is: $a_g = \gamma_I \, a_{gR}$ as shown in figure. 17. The importance factor γ_I = 1 is assigned to the reference return period $T_{RP,R}$ = 475 years.

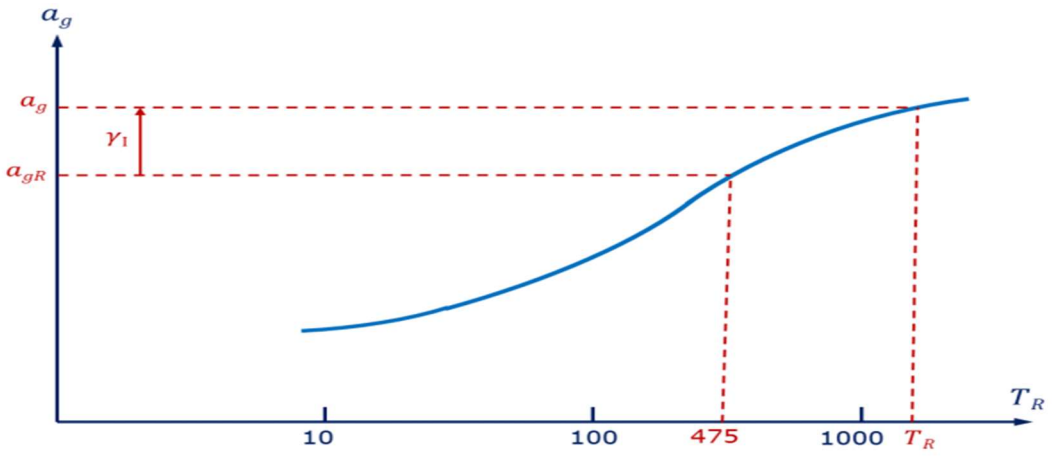

Figure 17 Calculation of γI according to EC8

Identification of ground types should be under consideration in the case of seismic design of the bridges and the average shear wave velocity Vs_{30} should be determined from Table 3.1 in EC8-1 (2004).

There are two types of the elastic response spectrum as shown in figure. 18. If deep geology is not accounted for, the recommended choice is the use of two types of spectra: Type 1 and Type 2. If the earthquakes that contribute most to the seismic hazard defined for the site for the purpose of probabilistic hazard assessment has a surface-wave magnitude, Ms, not greater than 5,5, it is recommended that the Type 2 spectrum is adopted.

For the five ground types A, B, C, D and E, the recommended values of the parameters soil factor S, lower limit of the period of the constant spectral acceleration branch TB, upper limit of the period of the constant spectral acceleration branch TC and beginning of the constant displacement response range of the spectrum TD are given in EC8-1 (2004) table 3.2 and 3.3.

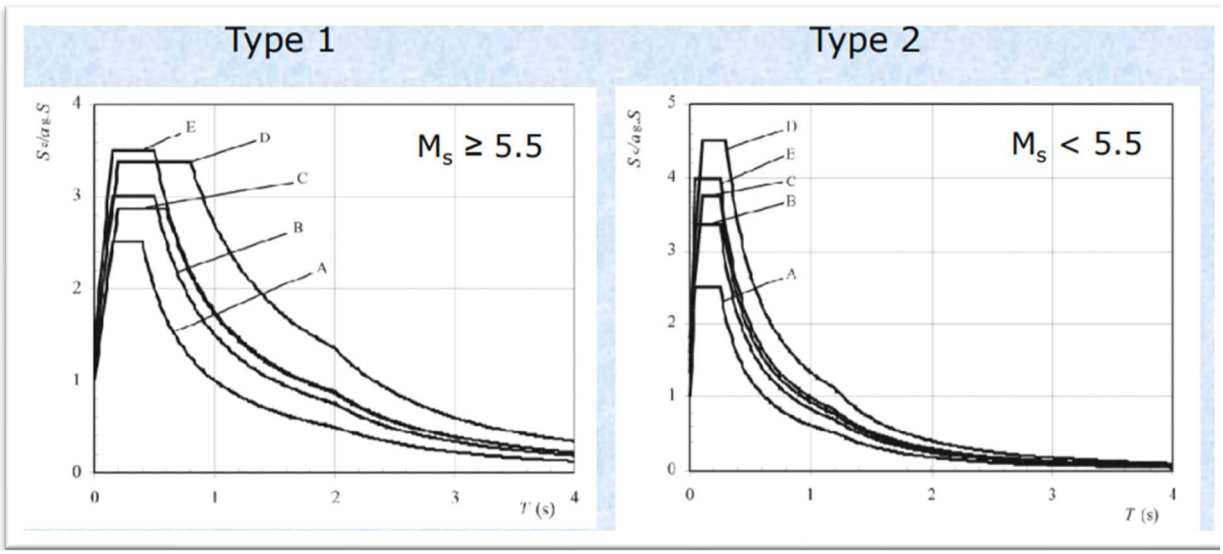

Figure 18 Recommended elastic response spectrums for ground types A to E (5% damping)

4.3 The effect of destroyed bearings on the behavior of the bridge in the presence of earthquakes

Although bearings or seismic isolation bearings can be a protective structural unit for the bridge superstructure of the damage during the seismic actions by playing a role to reduce the superstructure response to the existence excitation. The Last earthquakes investigations showed that the bearings between the multi span bridge superstructures girder and substructures are the weakest connection among the structure's resistance to seismic actions in many cases and it can cause more damage. It is proved that such bearings can be damaged due to the exceedance of inertia forces formed on the superstructure's girder, pounding forces between the adjacent vibration parts or forces which are transmitted between the superstructures and substructures [26].

After this damage, bearings are not able to hold the superstructure in a high-precision way as there are in a floating condition, also it causes increasing in the proportional displacement on the top of the abutments and that of course leads to exceed the probability of unseating failure for the main structure of the bridge and that what is investigated in Huilan Bridge damage during Wenchuan earthquake as shown in figure. 19.

Figure 19 Huilan Bridge damage during Wenchuan earthquake

By looking to Wenchuan earthquake which considered as the strongest earthquake occurred to china in [27],[28] , an investigation has been done to discover the damage failure types on multi span girder bridges and put design guideline to avoid these types of damage again. Various types of destruction have been detected, including girder collapse, damage in the expansion joints, pounding between the adjacent units, substructure abutments collapse, bearing displacement and sliding between the girder and the bearings which considered as the most common issue can cause the damage for the bridge in seismic actions.

From the damage study on Miaoziping Bridge which is located near the epicenter of the earthquake, it was found that there was no contact between the superstructure girder and the bearings due to the inertial forces on the girder which were larger than the friction forces in the connection between the bottom of the girder and the bearings and that caused sliding damage. Also, bearings in this case were located on a supporting concrete seat. So, when the relative displacements in the contact between the bearing and girder is larger than the seating width, it gave one more reason for unseating of the bridge span as shown in figure. 20 in addition to Gaoyuan Bridge and Naba Bridge which also suffered from unseating failure due to the inadequate seat width in figure. 21.

Moreover, by looking to Baihua Bridge, the presence of some adjacent girders that are based on the fixed bearings at different levels according to the different heights of abutments, which lead to the variation in the stiffness and dynamic characteristic and thus helped in the existence of large relative displacements in the span hinge in figure. 22. On the other hand, not much damage is observed to the abutments and the foundations of the bridges which means that girder sliding collapse can be an isolation system for the other units of the bridge.

Moreover, not much damage was observed to the abutments and the foundations the bridges which means that girder sliding collapse can be an isolation system for the other units of the bridge.

Figure 20 Span collapse of the Miaoziping Bridge

Figure 21 Girder failure for Gaoyuan Bridge and Nanba Bridge respectively.

Figure 22 Failure of the Baihua Bridg

Chapter 5 THE CASE OF STUDY

5.1 Introduction

As mentioned before about the effect of destroyed bearings on the behavior of the bridge in the presence of earthquakes and the damping properties of the CNT/polymer composites. CNT/polymer bearings with different weight fractions (5%, 4%, 3%, 2%, 1%) as structural components for seismic isolation were simulated using ABAQUS and used in the connection between bridge superstructure and substructure as a solution for the catastrophic failure in this connection during the earthquake events. Then, trying to get the assessment by checking the superstructure to substructure connection, checking the moment at the base of the piers, and comparing that to the case of the bridge without these bearings types as the connection between the superstructure and substructure is monolithic as explained before.

5.2 Carbon nanotubes polymer composite multiscale modeling

For the accurate description of the CNT/polymer composite material and to extract accurate stress-strain curve as mentioned before, a multiscale model with three stages is implemented. The atomic scale is linked with the microscopic scale with a hierarchical approach, while the microscopic is linked with the macroscopic scale with a semi-concurrent approach.

5.2.1 Microstructure formulation

At the atomic scale, the modified molecular structural mechanisms (Mmsm) method was used to model each pair of carbon's C-C covalent bonds. The lattice was simulated as a space frame structure, where every bond between adjacent atoms was modeled as a continuous circular

beam and this way of simulation is fairly accurate. However, it led to excessive computational cost for each CNT, and thus, before proceeding to the next scale each space frame was projected to an equivalent beam element (EBE), which reduces the total degrees of freedom of the structure to a reasonable amount.

The structural properties of the EBEs were calculated by subjecting a cantilever beam to an axial F_x, a transverse F_y and a torsional T load, as illustrated in figure. 23. Subsequently, the axial stiffness $(EA)_{eq}$, the bending rigidity $(EI)_{eq}$ and the torsional rigidity $(GI)_{eq}$ were obtained by measuring the horizontal displacement u_x, the vertical displacement u_y and the angle of rotation ϕ corresponding to the aforementioned loads from the following load-deflection relations:

$$(EA)_{eq} = \frac{Fx\, L0}{Ux}\,, (5\text{-}1)$$

$$(EI)_{eq} = \frac{Fy\, L_0^3}{3\, Uy}\,, (5\text{-}2)$$

$$(GI)_{eq} = \frac{T}{\phi} L_0\,, (5\text{-}3)$$

where L0 is the beam's length.

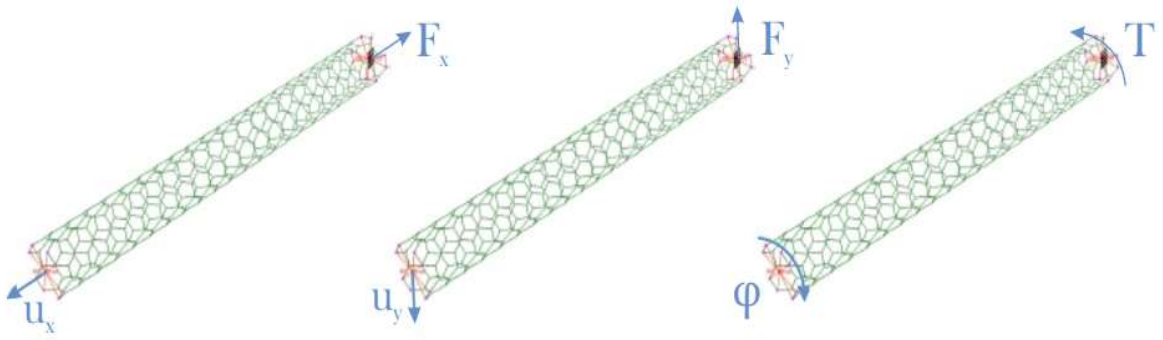

Figure 23 mMSM model of a CNT subjected to three deformation cases.

At the microscopic scale a representative volume element (RVE) was chosen for the formulation of the surrounding polymer matrix. A number of EBEs were then added as inclusions of the matrix in order to achieve a specific volume fraction of CNT/polymer.

5.2.2 **Homogenization Scheme**

Before the transition to the macroscopic scale, a homogenization scheme must be implemented towards a connection with the microstructure.

This scheme was applied to the microscopic model of an RVE of polymer matrix and linear EBEs representing the CNT reinforced inside the matrix. According to it, for a given macroscopic strain $\bar{\varepsilon}$ a linear displacement function was applied to the boundary of the RVE as:

$$u(x) = \bar{\varepsilon}\, x \text{ at } x \in \partial V, \quad (5\text{-}4)$$

where x is the position vector of a point on the boundary ∂V of the RVE. This relation provides the boundary conditions that are applied to the RVE with respect to the macroscopic variable and is referred to as the localization rule.

The solution of the aforementioned boundary value problem will produce the macroscopic stress $\bar{\sigma} = [\ \bar{\sigma}_{11}\ \bar{\sigma}_{22}\ \bar{\tau}_{12}\ ]^T$, calculated by the volume average of the microscopic stress field $\sigma\ (x)$ via the relation:

$$\bar{\sigma} = \frac{1}{\|V\|}\ \text{sym}\ (\int_v \sigma\ dx), \quad (5\text{-}5)$$

with $\|V\|$ denoting the volume of the RVE. This equation expresses the homogenization rule, which yields the macroscopic state variables as a function of the microscopic stress state. The

transition from the microscopic level to macroscopic and vice versa is schematically presented in figure. 24.

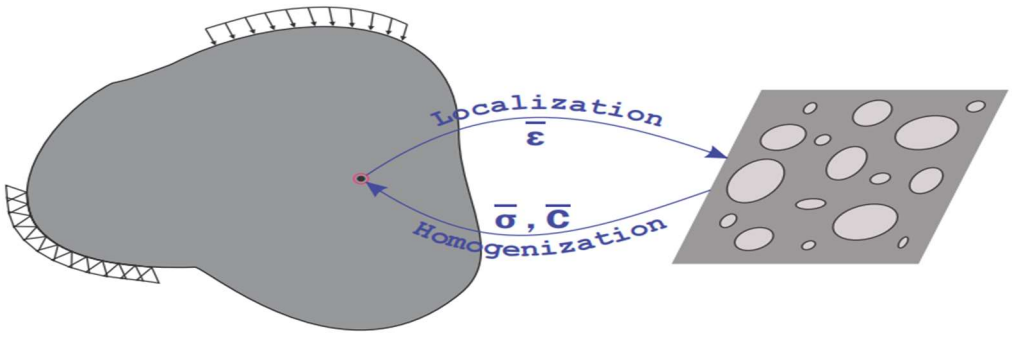

Figure 24 Transition between scales during FE²

Lastly, the macroscopic tangent (effective) modulus $\bar{C}$ is calculated as the derivative of the macroscopic stress $\bar{\sigma}$ with respect to the macroscopic strain $\bar{\varepsilon}$, that is:

$$\bar{C} = \partial \varepsilon \, \bar{\sigma} \, , \quad (5\text{-}6)$$

In the context of the finite element method, the above equations can be recast in matrix form as follows. After discretizing the RVE, linear displacements were imposed on the boundary nodes according to the macroscopic strain $\bar{\varepsilon}$ (localization rule) with the following relation:

$$U_n = D_n \, \bar{\varepsilon} \, . \quad (5\text{-}7)$$

5.3 Abaqus simulation

5.3.1 Bridge geometric simulation

For the bridge, which is the case of study, as shown in figure. 25 consists of three spans, the length of the first and last span is 16.6 m while the middle span length is 19.35 m. The deck section is a combination of a solid part and hollow section part. To simplify the model, the solid part has been replaced with a hollow section part while maintaining a constant weight of the

bridge as shown in figure. 26. All the abutments are 4.3 m width and 0.9 m thickness with different heights as shown in figure. 25. The connection between the abutment and the deck once is monolithic and another through bearings as shown in figure.27. Bearings are assumed 60 cm* 20 cm with 40 cm thickness.

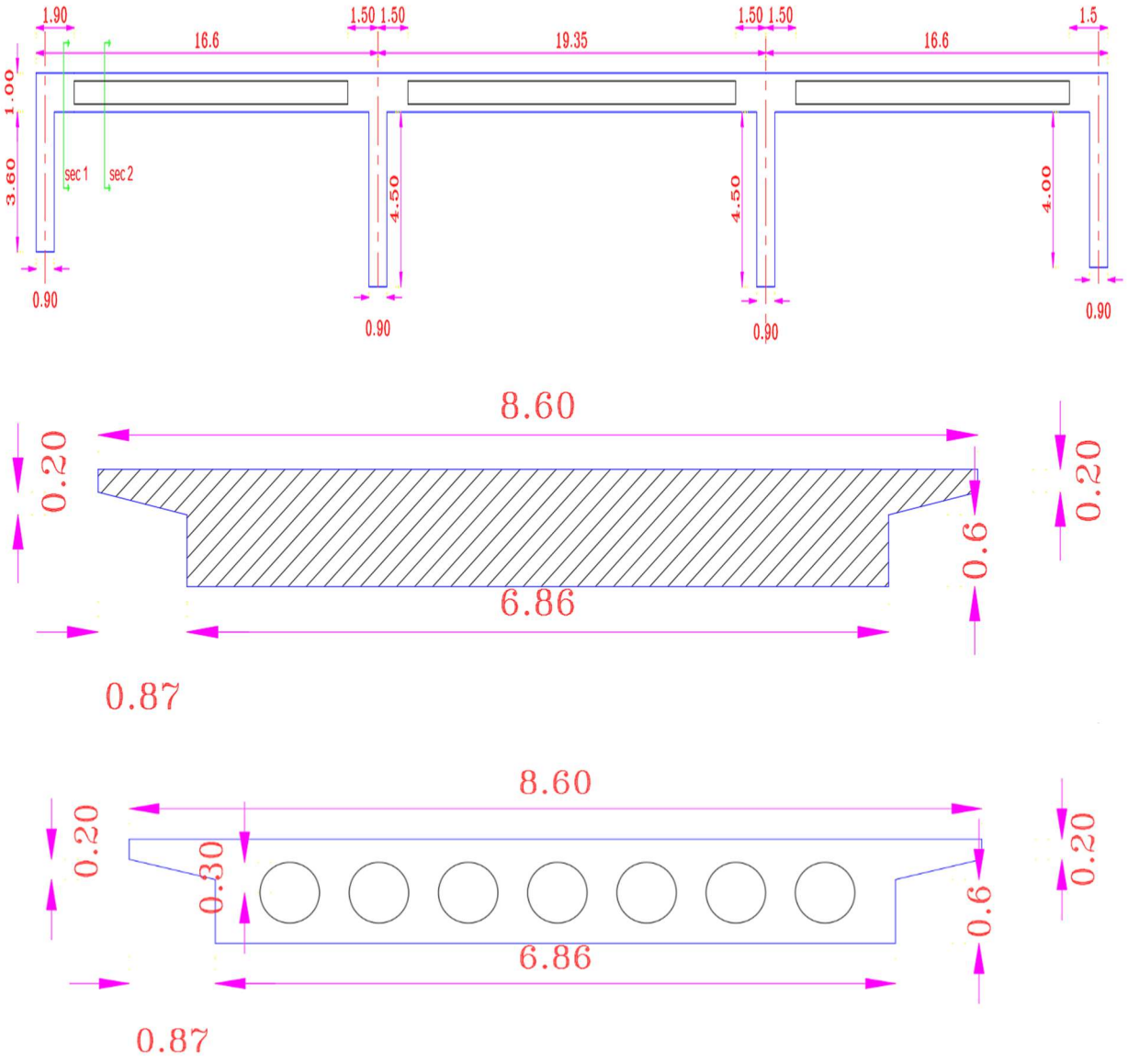

Section 2

Figure 25 The bridge layout.

Solid part length*Solid section area = Hollow part length* Hollow section area

$3m * 7.352m^2 = x_1 * 5.25m^2$

$X_1 = 4.2m.$

Total span length = hollow span length + x_1

First and last span length = 13.6+4.2 = 17.8 m.

Middle span length = 16.35+4.2 = 20.55m.

Figure 26 Calculations of replacing the solid section part with hollow section.

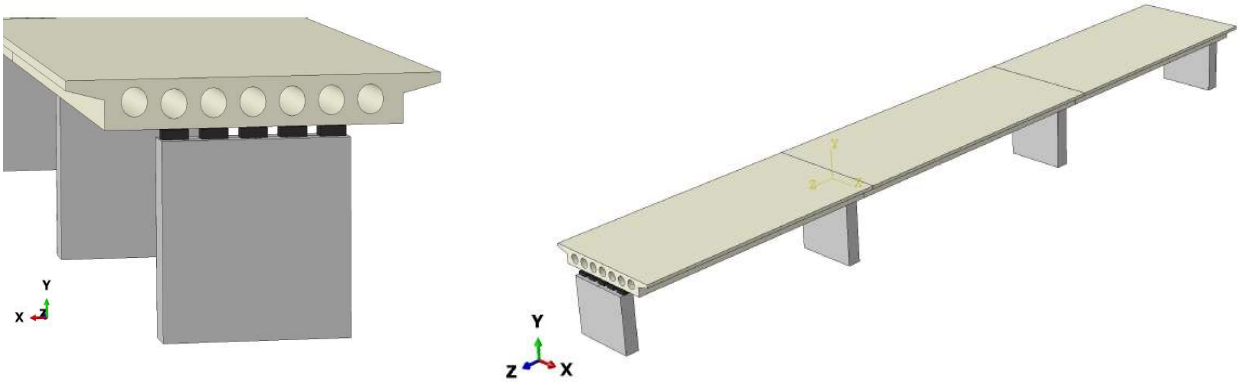

a) Connection through bearings

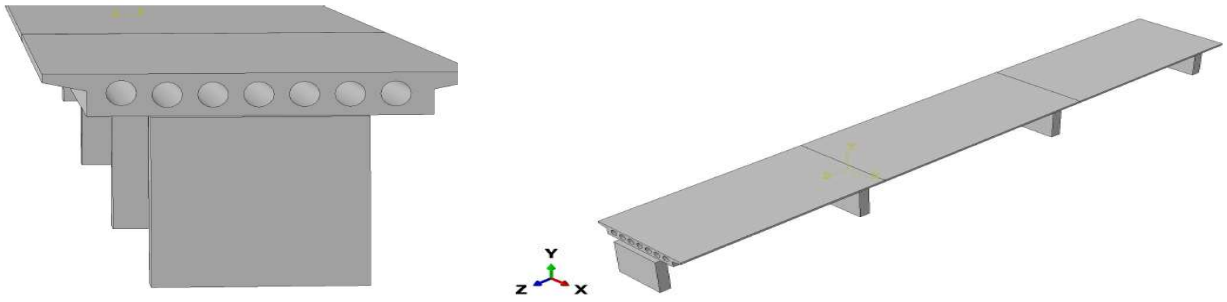

b) monolithic connection

Figure 27 Abaqus bridge simulation

5.3.2 **Interaction behaviour between parts**

For the interaction between decks and abutments in a case and the contact between bearings, abutments and decks in another case, surface to surface contact has been defined with friction factor equals 1 to prevent any sliding as shown in figure. 28 in addition to fixed ties has been define to prevent any rotations.

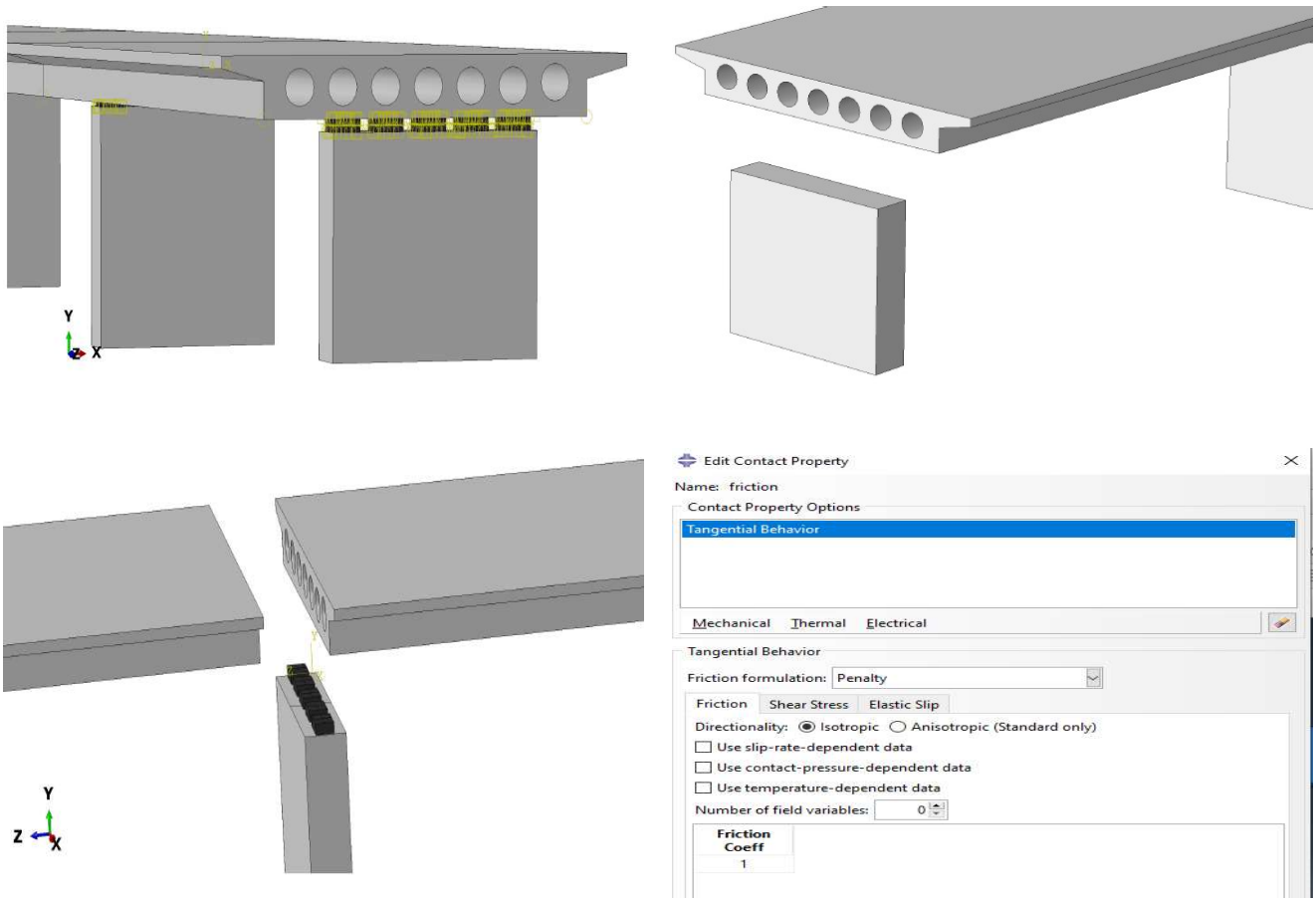

Figure 28 Interaction between each part.

5.3.3 **Load case**

Load case has been applied according to the EN 1998-2:2005 as shown in figure. 29. The load case is simply a combination between the dead load which was presented by the own weight in addition to the live load which is presented by the traffic load multiply by a factor depending on the type of the bridge which is road bridge in this case as shown in figure. 30, plus the seismic load which has been defined by time history Northridge as shown in figure. 31.

Traffic loads have been calculated according to Eurocode as shown in figure. 32.

5.5 Combination of the seismic action with other actions

(1)P The design value E_d of the effects of actions in the seismic design situation shall be determined in accordance with EN 1990:2002, **6.4.3.4** and EN 1998-1:2004, **3.2.4(1)** as:

$$E_d = G_k \text{ "+" } P_k \text{ "+" } A_{Ed} \text{ "+" } \psi_{21} Q_{1k} \text{ "+" } Q_2 \qquad (5.4)$$

where:

"+" implies "to be combined with";

G_k are the permanent actions with their characteristic values;

P_k is the characteristic value of prestressing after all losses;

A_{Ed} is the design seismic action;

Q_{1k} is the characteristic value of the traffic load;

ψ_{21} is the combination factor for traffic loads in accordance with **4.1.2(3)**P; and

Q_2 is the quasi-permanent value of actions of long duration (e.g. earth pressure, buoyancy, currents etc.)

Figure 29 EN 1998-2:2005 load combination.

Bridges with severe traffic and for the UDL system of Model 1 (LM1)

Road bridges $\psi_{2,1} = 0,2;$

Railway bridges $\psi_{2,1} = 0,3.$

Figure 30 Combination factors for traffic loads

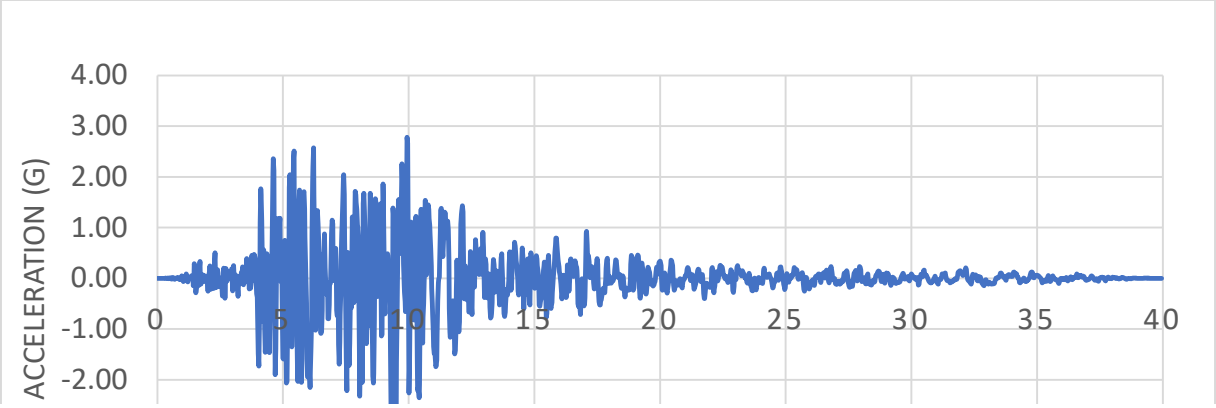

Figure 31 Northridge seismic time history

Total area of the bridge = 481.2 m2
Traffic vehicle = $\frac{60+40+20\ ton}{481.2}$ = .2493 ton/m2 = 2.493 kn/m2
Distributed load = (2.5+9) kn/m2*lane width (3 m) *(lane length (56.15m)) = 1937.175 kn
Distributed load = $\frac{1937.175}{481.2}$ = 4.025 kn/m2
Total load = 4.025+2.493 = 6.518 kn/m2

Figure 32 Traffic load calculations according to the Eurocode

5.3.4 **Boundary conditions**

For the case of study, fixed supports have been applied in Y and Z directions to prevent the movement at the base of the bridge abutments while x is still free under the effect of the seismic load as shown in figure.33.

To define the boundary condition of seismic effect in x direction, time history should be defined as mentioned before and after, acceleration or angular acceleration should be selected as shown in figure.34.

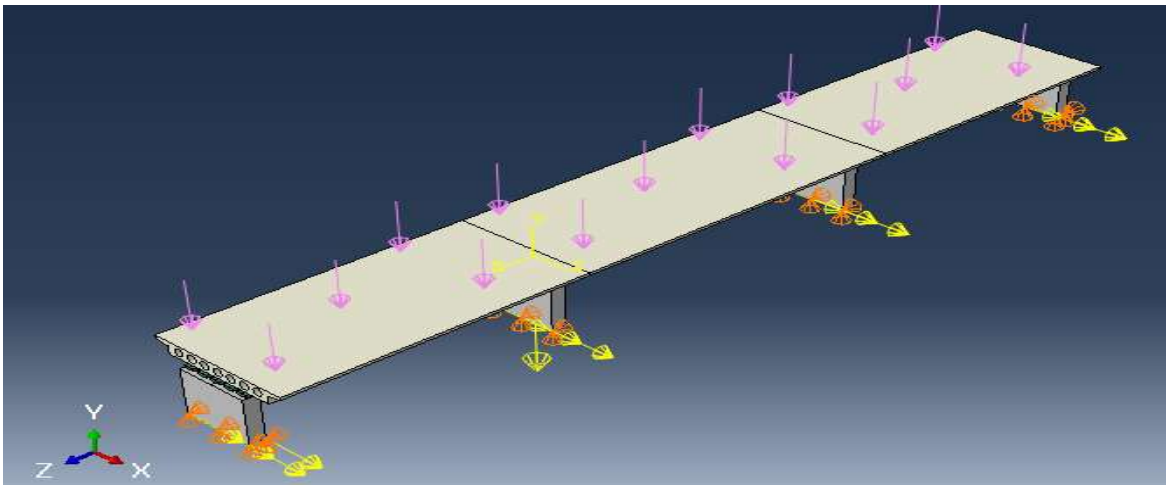

Figure 33 Boundary conditions added to the bridge model

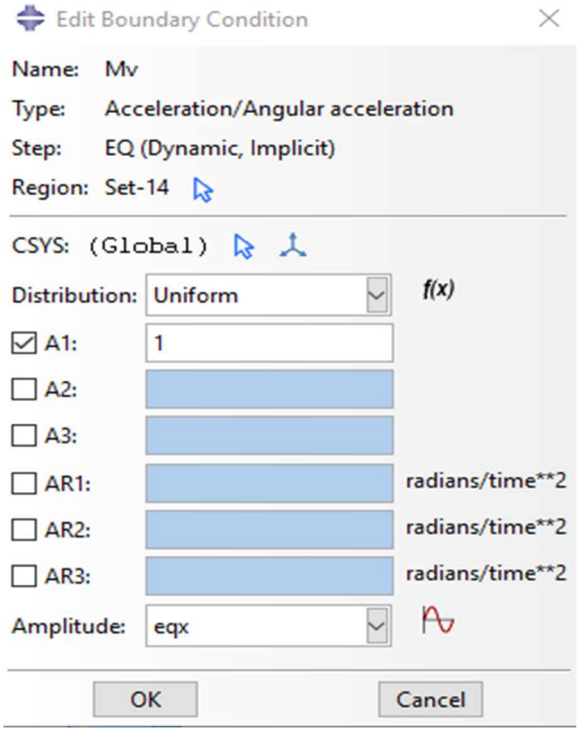

Figure 34 Acceleration or angular acceleration boundary condition

5.3.5 **Material definition**

5.3.5.1 **The Pier and deck material**

Concrete 40/50 according to the EN 1992-1-1 has been defined for the deck bridge as the modulus of elasticity E = 35000000000 N/m^2 , Poisson's ratio = 0.2 and mass density = 2548.5. While for the pier material definition, the modulus of elasticity has been reduced to

10500000000 N/mm^2 , to be equal 0.3 of the modulus of elasticity of the deck to allow the first plastic hinge to be at the pier.

5.3.5.2 **Numerical simulation for CNT polymer composite**

polymer matrix reinforced with straight, unidirectional CNTs was analyzed. The polymer matrix and the CNTs were considered linearly elastic. The matrix is composed of polyether-ether-ketone (PEEK), whose elastic modulus and Poisson's ratio are 2 Gpa and .4 respectively. The nanotubes are single-walled with outer diameter 1.063 nm.

A small portion of a nanotube was modeled as a space frame, using mMSM. The resulting model was then projected on an EBE with a pipe profile section whose wall thickness was chosen as tf = 0.34 nm to reduce the total degree of freedom of the structure. The EBE's mean equivalent length and Young's modulus are 50 nm and 1051Gpa respectively.

Then, a RVE was modeled, which consisted of a single CNT embedded in a square PEEK matrix. The RVE finite element model is 100nm width, 100 nm height and thickness 20 nm, the matrix is discretized with plane stress finite elements and the CNT with truss elements, having the properties of the previously derived EBE. Several CNT weight fractions were considered, ranging from 1 to 5 %, which were obtained by varying of the CNTs according to the relation,

$$\text{Weight fraction} = \frac{\text{number of CNT} * \text{CNT area} * \text{CNT length}}{\text{total volue of the RVE}} .$$

Finally, extracting the stress strain curve of each weight fraction case as shown in figure.35.

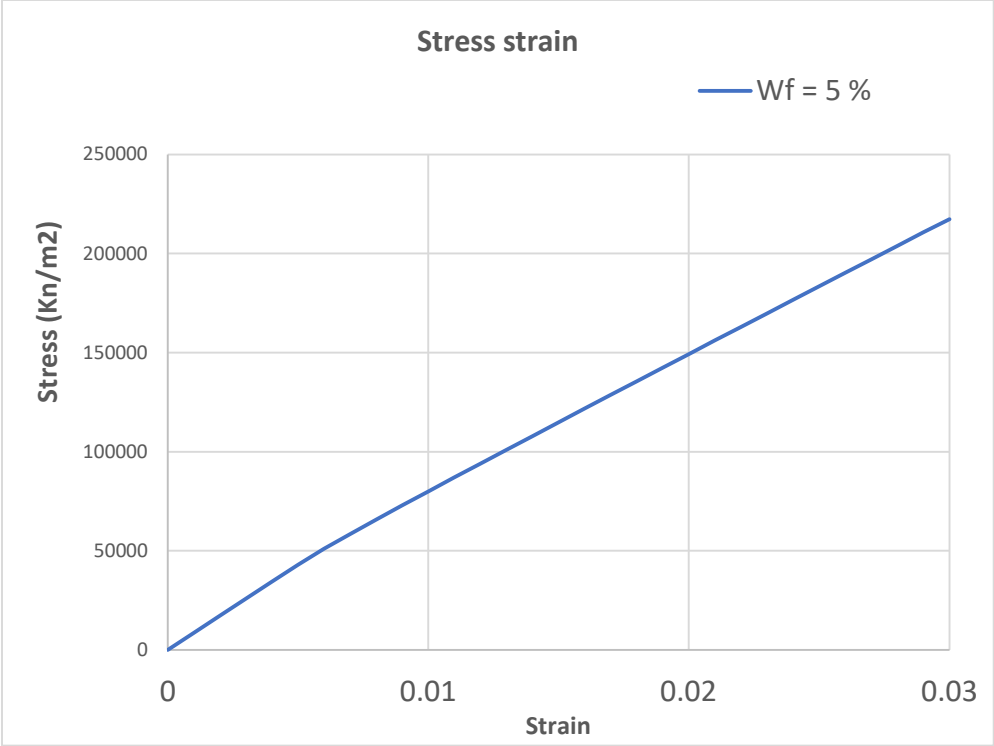

a) Number of CNTs = 176.

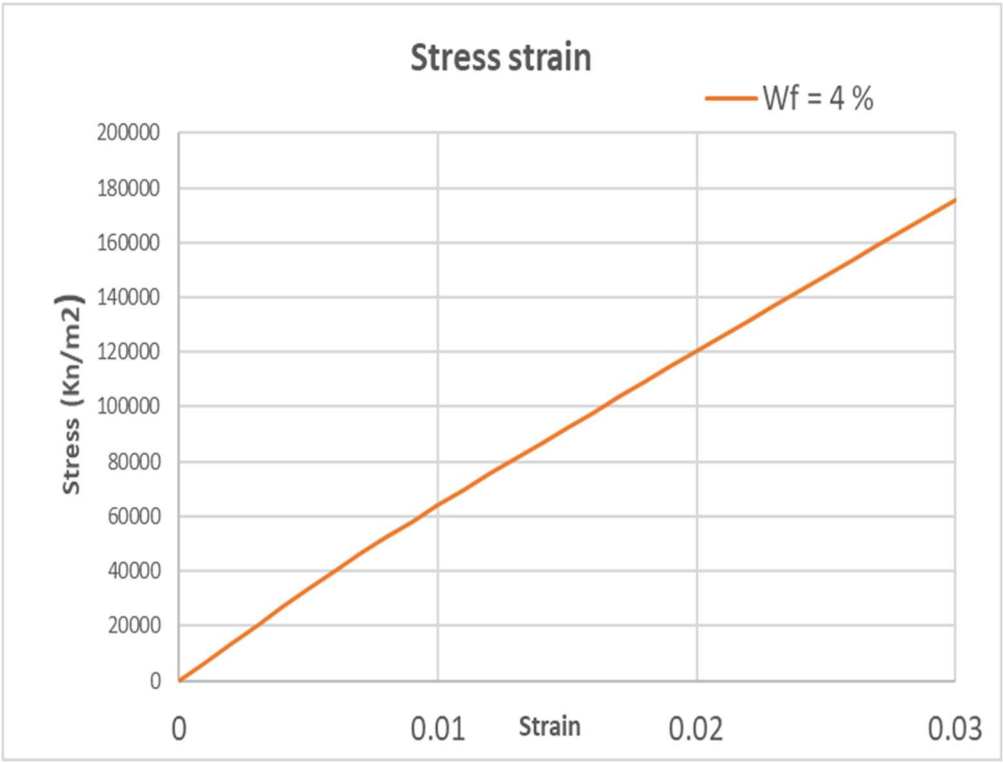

b) Number of CNTs = 141.

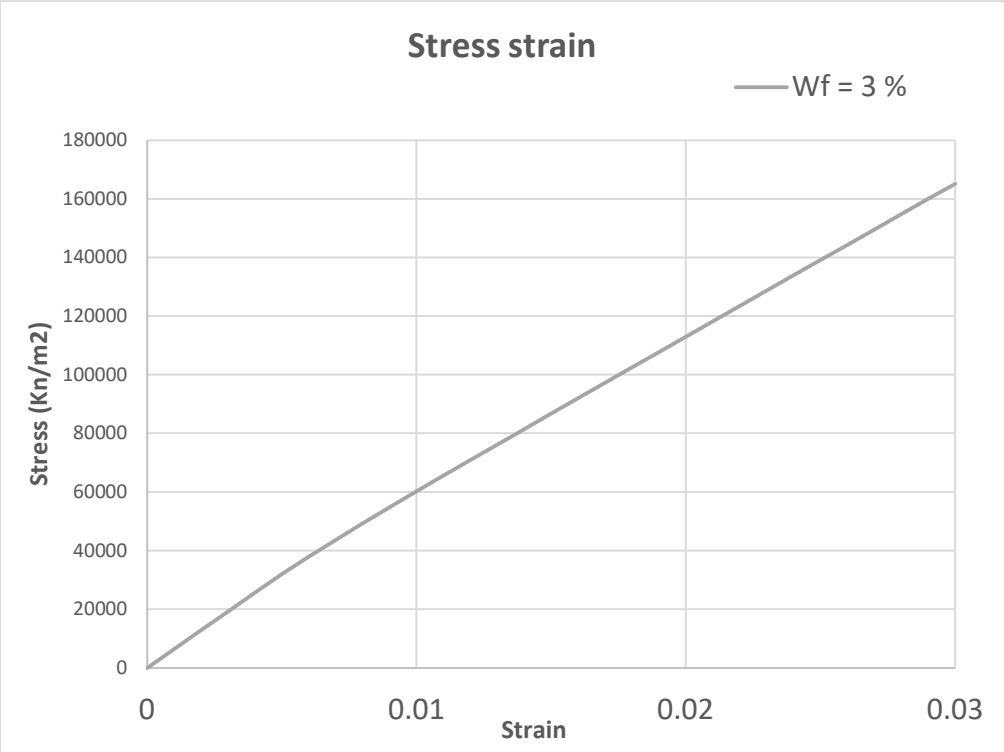

C) Number of CNTs = 106.

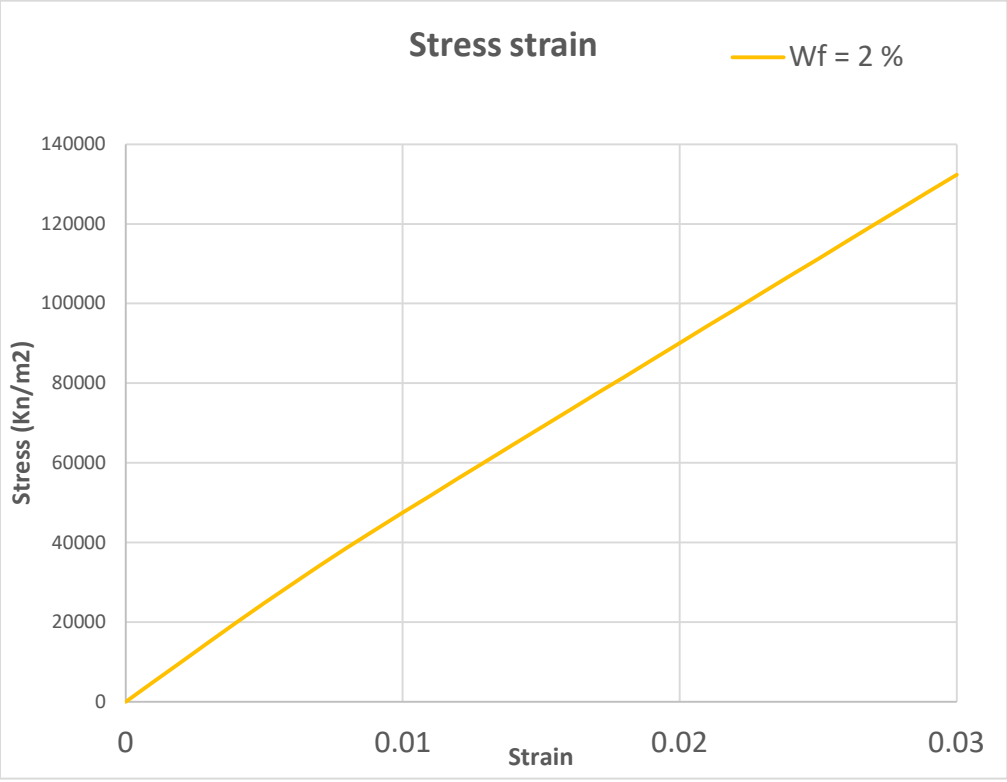

D) Number of CNTs = 70.

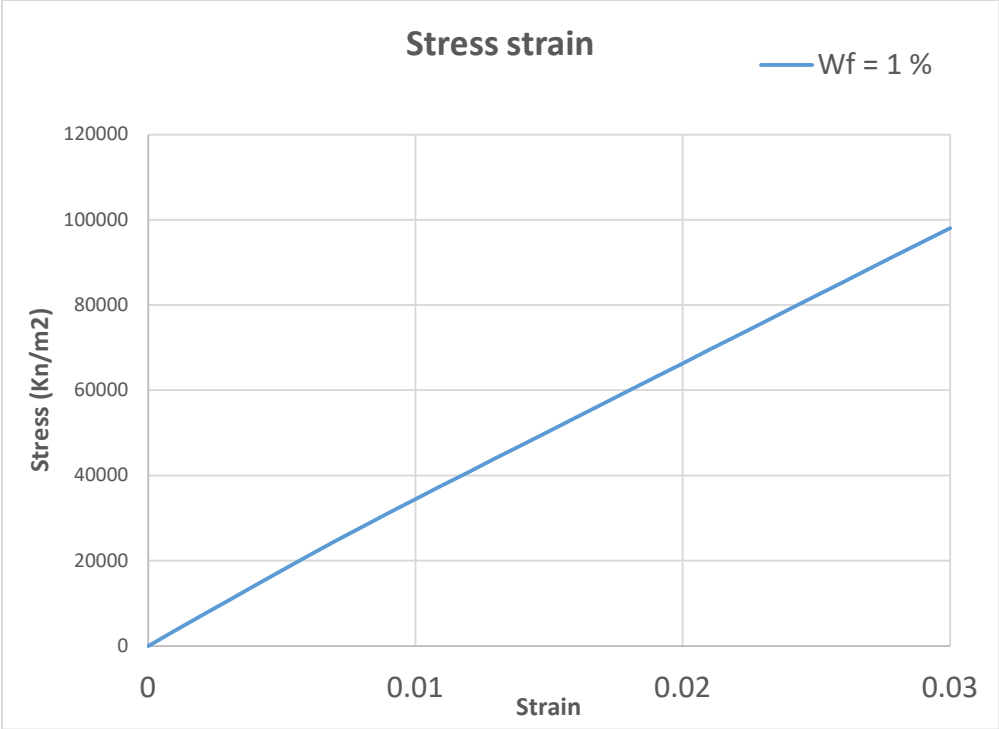

E) Number of CNTs = 35

Figure 35 Stress – strain curve for each weight fraction.

5.3.5.3 **Bearing's material**

After extracting the stress and stain curve for each weight fraction as explained in previous, material has been defined by calibration as shown in figure. 36.

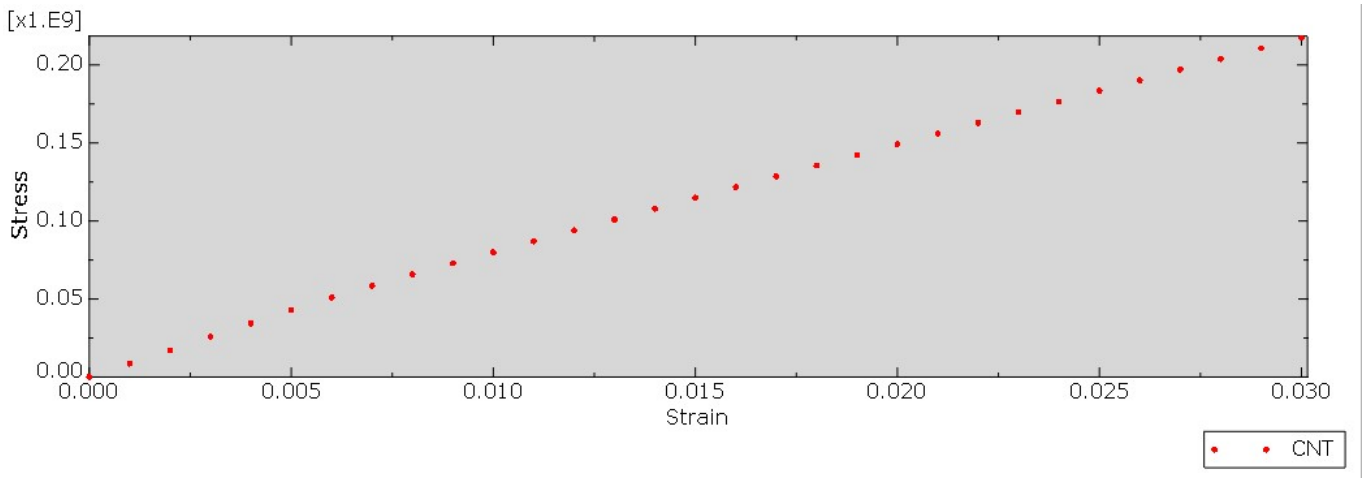

a) defining stress-strain curve for 5 % wf.

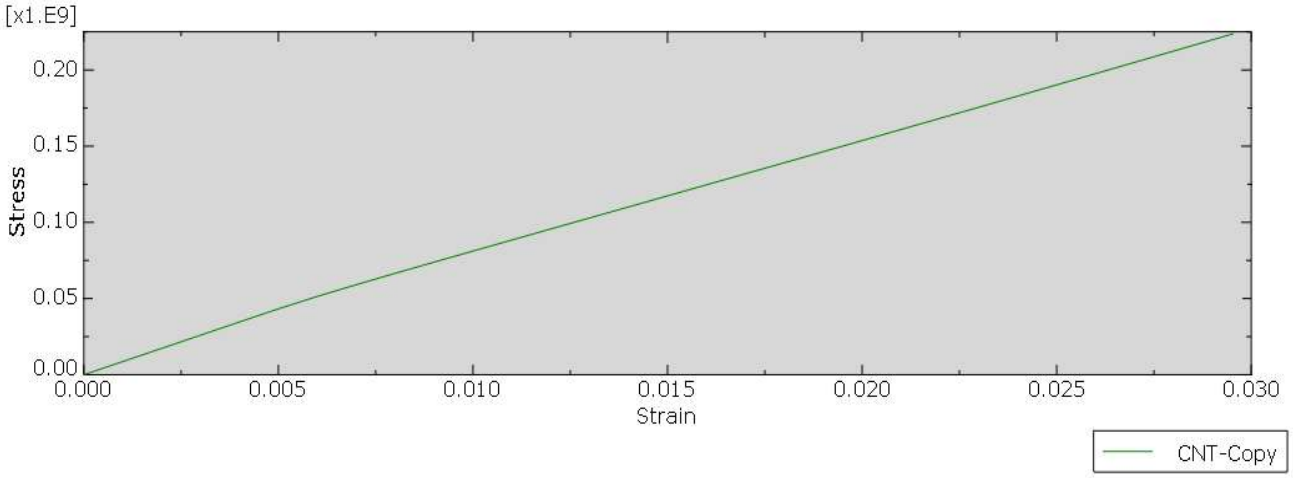

b) selecting yield point and ultimate point

Figure 36 CNT/polymer composite calibration definition

5.4 Earthquake assessment

5.4.1 Calculating the time period of each structure

To monitor the effect of the bearings in each case for seismic isolation and comparing that to the case of the bridge with monolithic connection (no bearings). Time period has been calculated for each structure by using the function,

$$T = 2^{*} \Pi * \sqrt{\frac{m}{k}},$$

Where m is the mass of the structure which equals 962083 N, K is the stiffness of the structure which equals $\frac{1}{Ux}$, Ux is the displacement of the bridge in X direction (earthquake direction) due to 1 N force as shown in figure.37.

The time period of each structure has been determined as shown in figure.38 and has been signed on the response spectrum chart of the earthquake as shown in figure. 39.

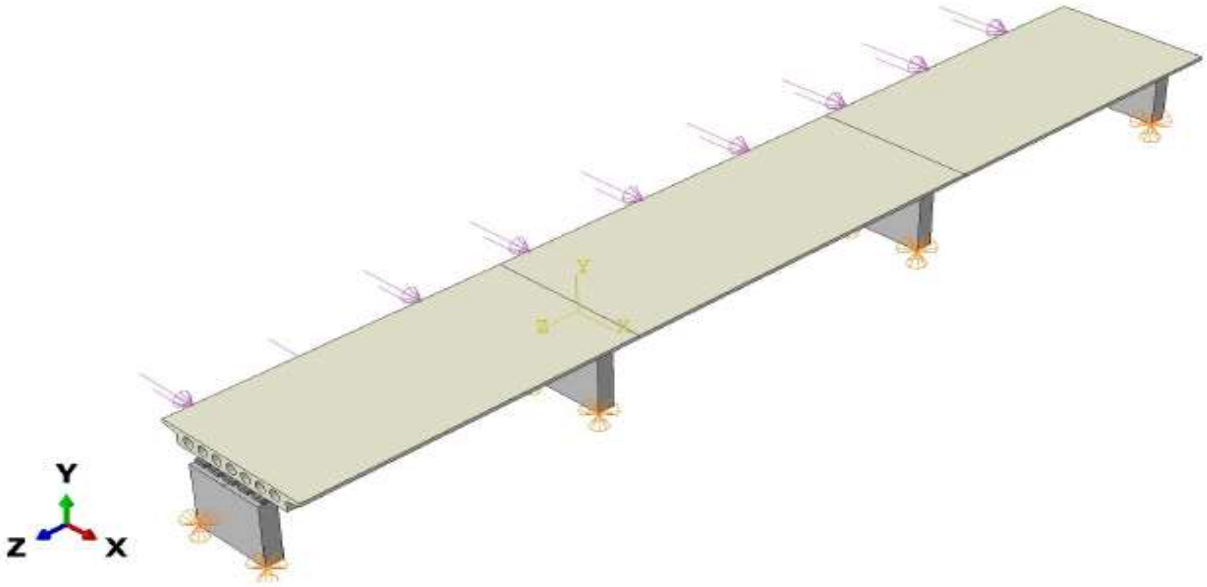

Figure 37 calculating displacment according to 1N in x dirction.

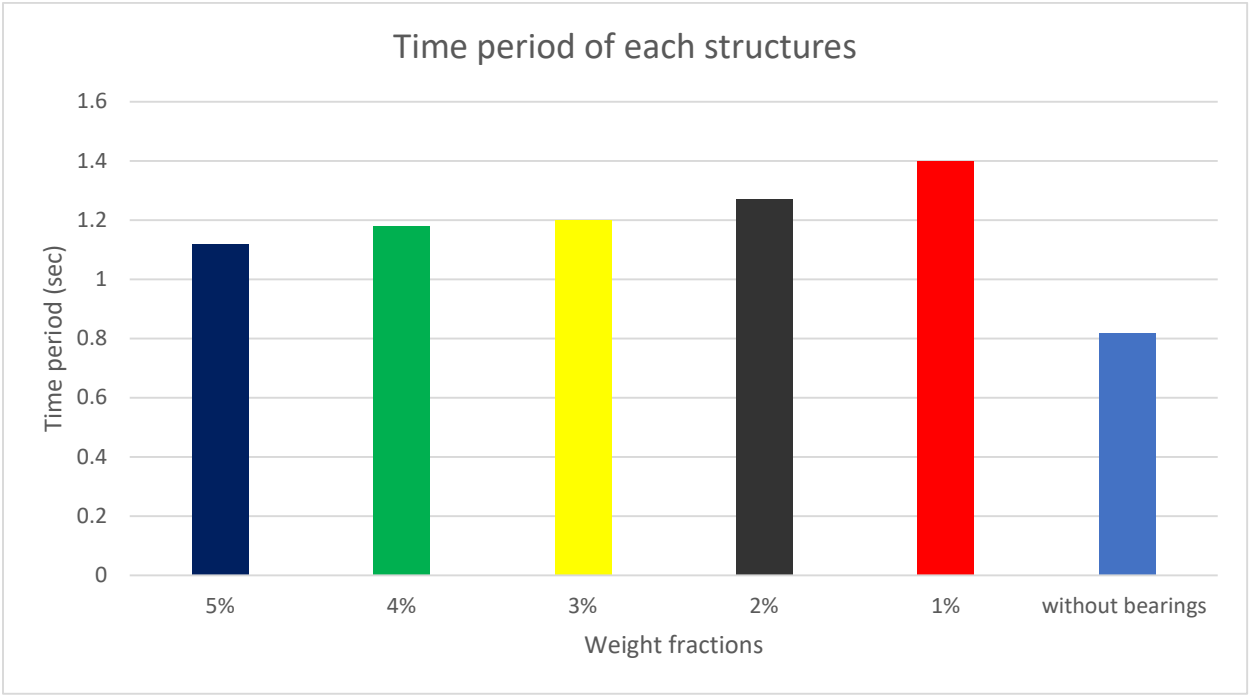

Figure 38 Time period of each structure

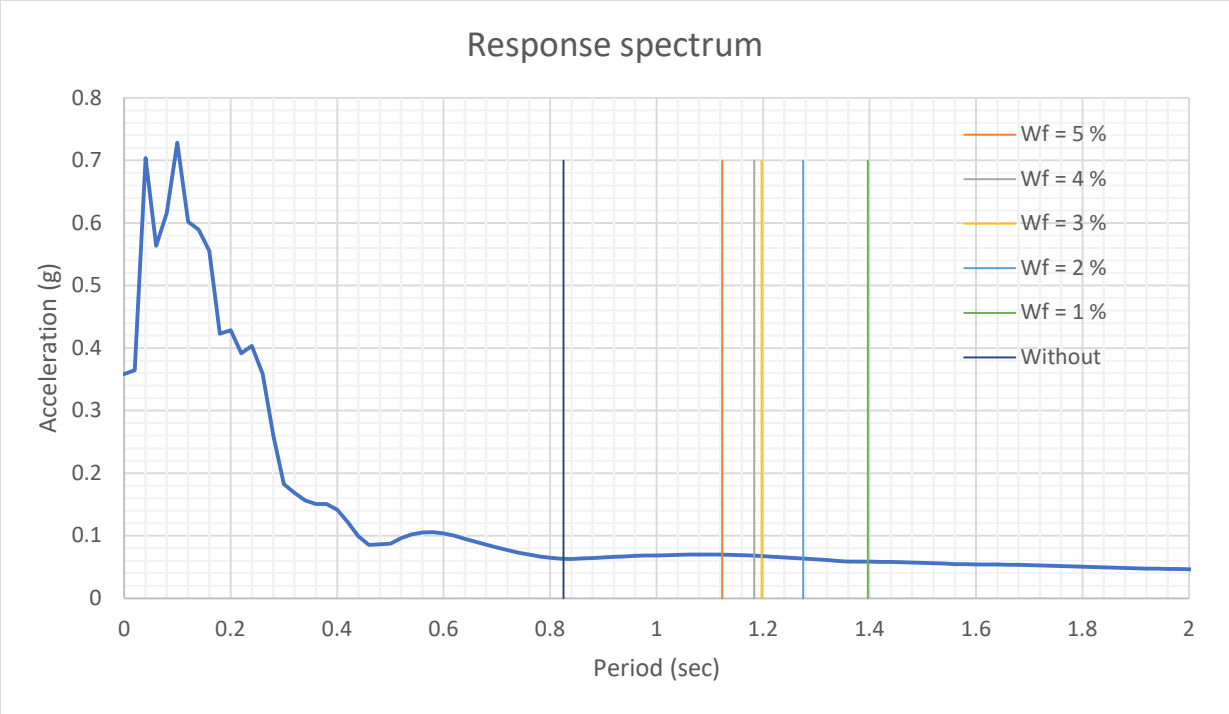

Figure 39 the time period of each structure locating on the response spectrum chart of earthquake.

5.4.2 **Check superstructure to substructure connection**

After checking the time period of each structure. Calculation for the shear strains of the middle bearing with different weight fraction at each time period have been calculated by using the function,

$$\gamma = \frac{U2-U1}{h},$$

Where U2 is the displacement of a point locating upper the bearing on the deck of the bridge, U1 is the displacement of a point locating lower the bearing on the abutment of the bridge and h is the height of the bearings.

Results are illustrated in figure. 40, for the 39.94 seconds of the earthquake time history. While figure. 41 and 42 shows the shear strain for the first 10 seconds and 20 second of the earthquake time history respectively which regards the most effective time for the earthquake.

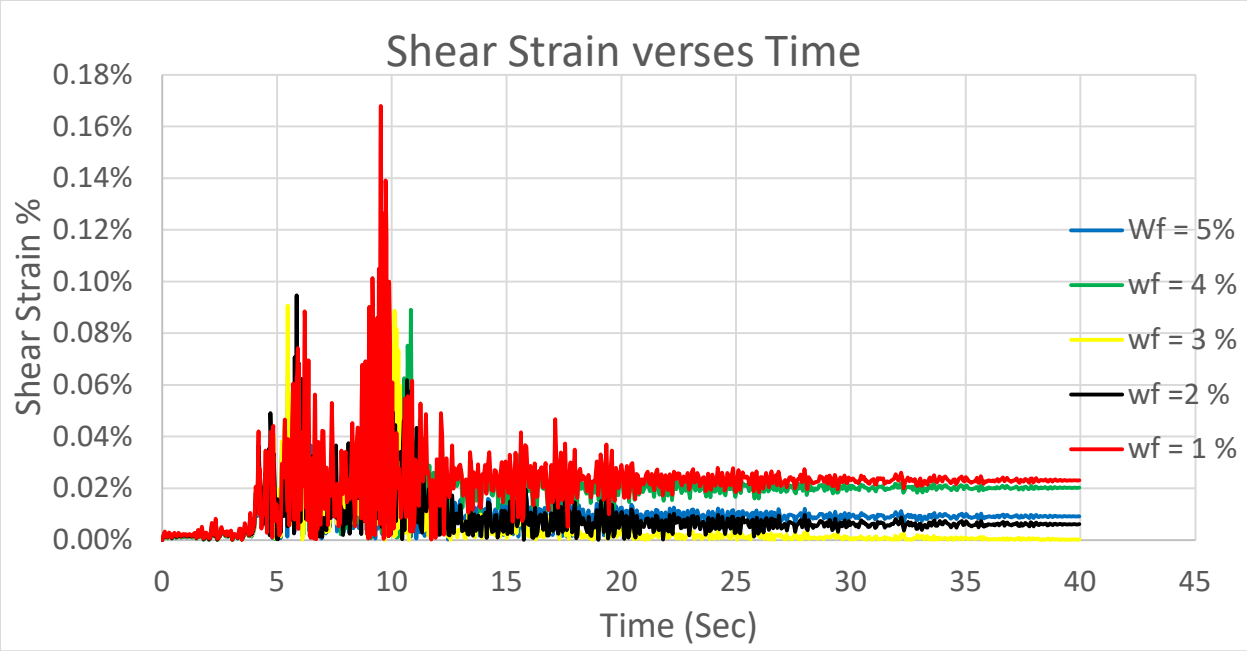

Figure 40 shear strain of each structure for 39.94 seconds of the earthquake

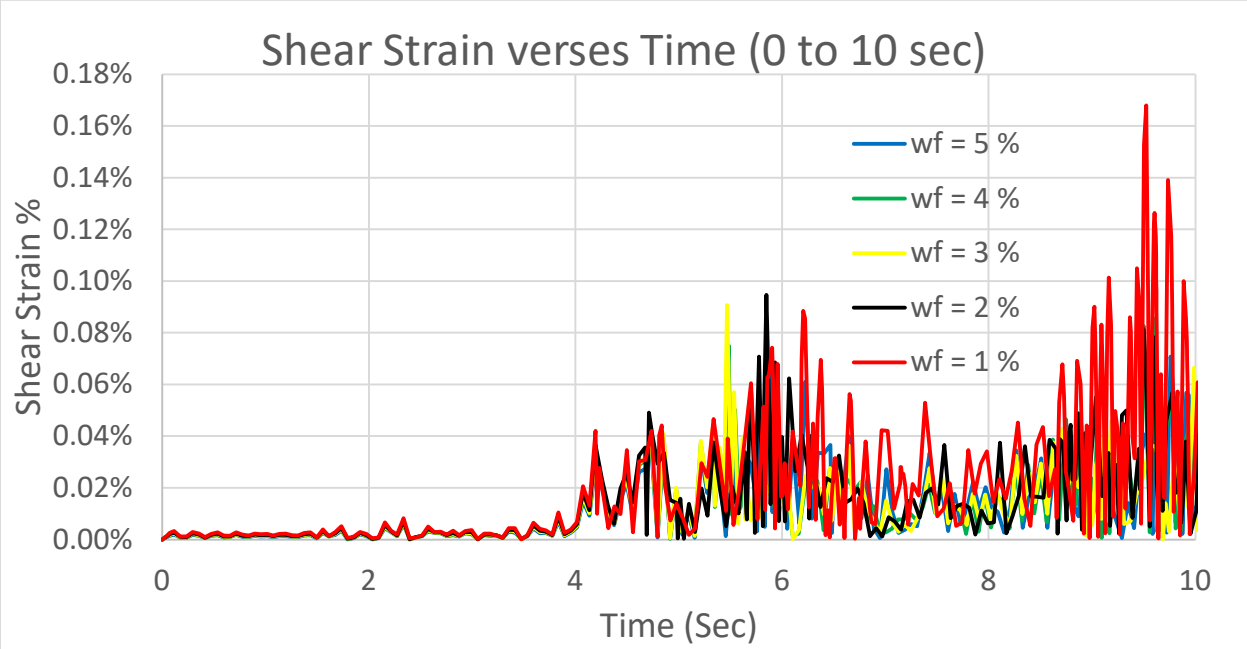

Figure 41 Shear strain of each structure for the first 10 seconds of the earthquake

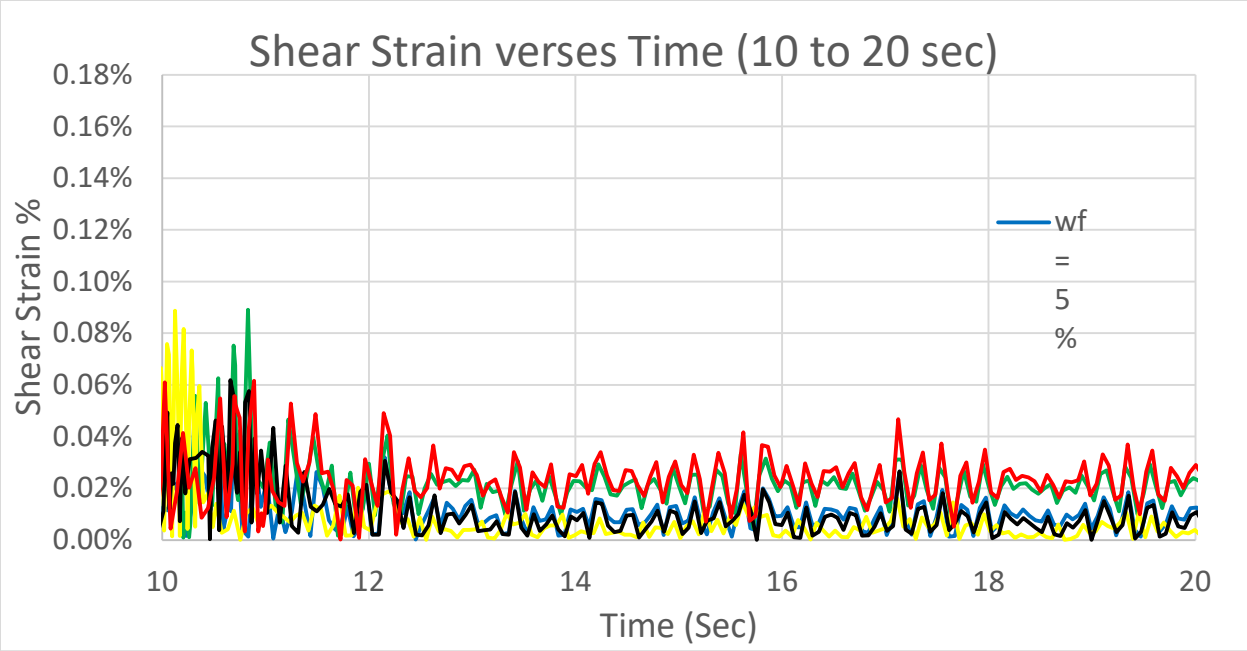

Figure 42 Shear strain of each structure for the period between 10 to 20 seconds of the earthquake

5.4.3 **Check the bending moment at the base of the piers**

To compare the effectiveness of the different bearings for seismic isolation and compare them to the case of the bridge without bearings, bending moment has been monitored at a point on the base of one pier for each time period as shown in figure. 43, 44 and 45.

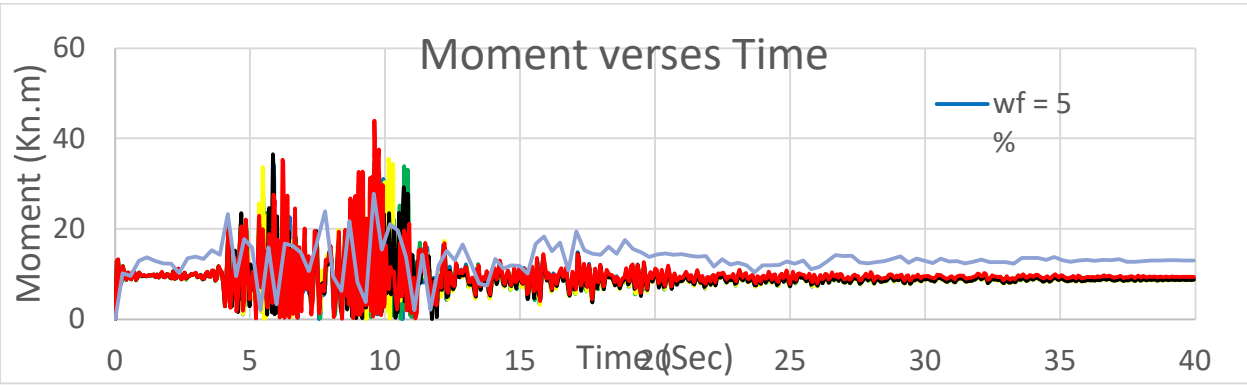

Figure 43 Bending moment of each structure for 39.94 seconds of the earthquake

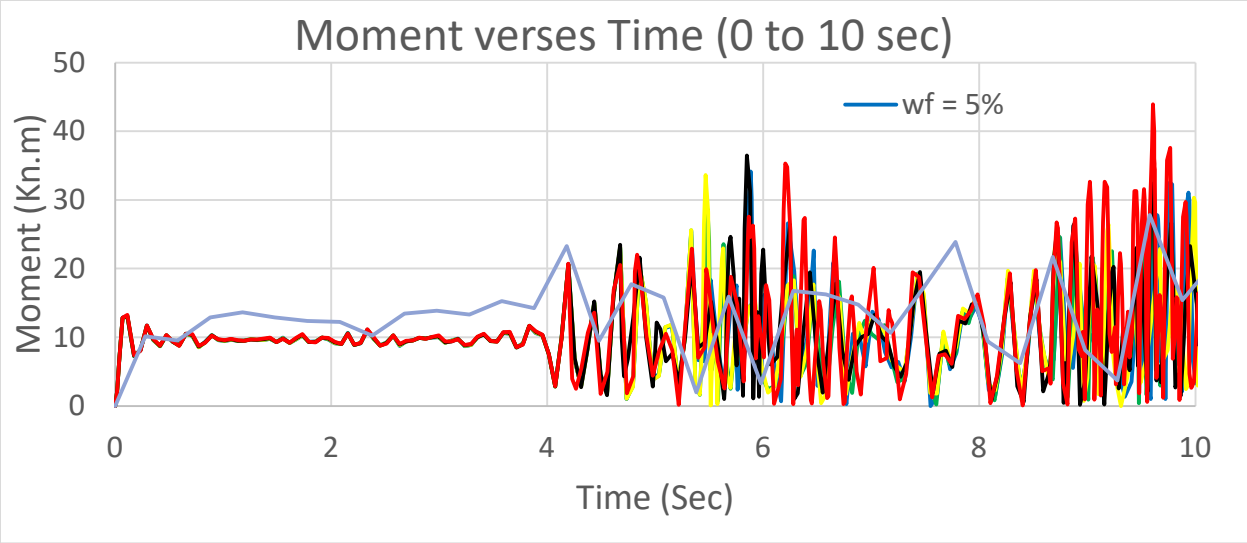

Figure 44 Bending moment of each structure for the first 10 seconds of the earthquake

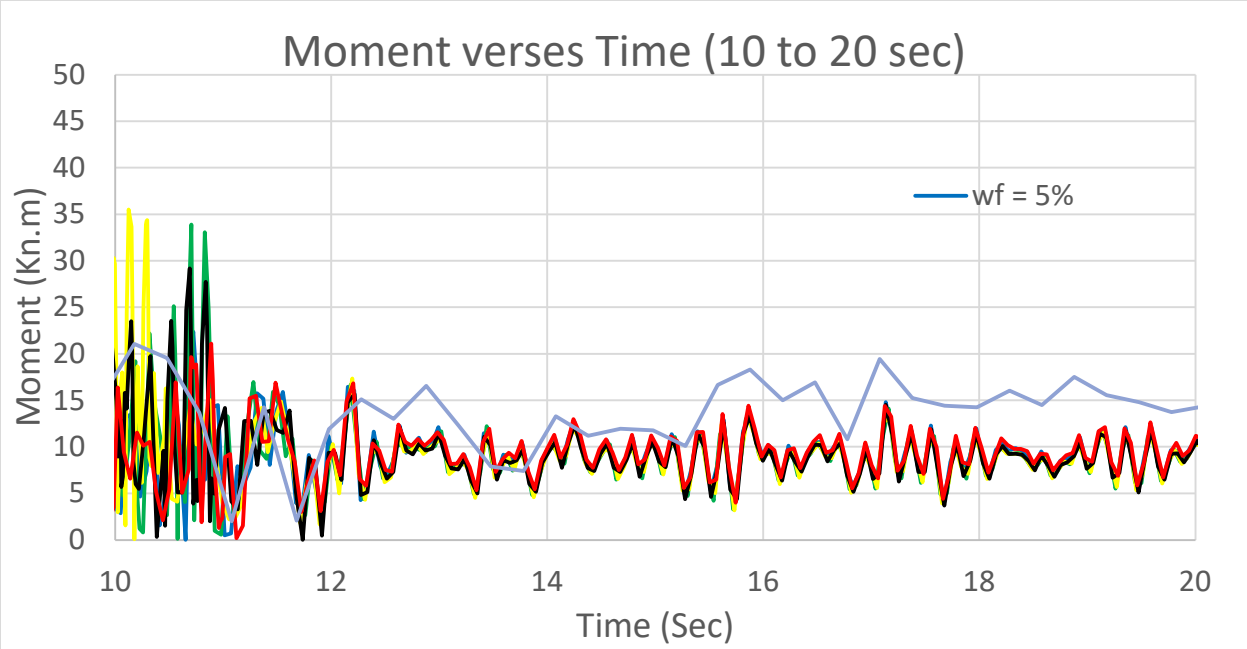

Figure 45 Bending moment of each structure for the time between 10 to 20 seconds of the earthquake

Chapter 6 CONCLUSIONS AND FURTHER WORK

6.1 Conclusions

According to the previous simulation attempts for CNT/polymer composite, it is clear that higher values of CNT weight fraction will give more damping properties. On the other hand, ISS increase the stiffness and decrease the damping significantly. In addition, to improve damping properties of the structure, an optimum extent of microstructural slippage has to be achieved. Higher weight fraction can yield larger damping if ISS is low enough to achieve the optimum slippage. Increasing the amplitude of the load applied will increases the ISS for which the damping ratio is maximized.

It can be noticed that an increase of the time period of the bridge has been achieved by using the CNT/polymer bearings as it increased from 0.82 seconds in the case of the no bearings in the connection between the superstructure and substructure to 1.4 seconds in the case of using bearings with 1 % weight fractions, which mean more seismic isolation for the bridge structure.

It can be also noticed that increasing the weight fraction is decreasing the time period of the structure re and it is expected as the increasing of the weight fraction is decreasing the stiffness and thus the structure time period as mentioned before.

On the other hand, it can be observed that there is no obvious difference in shear strain and bending moment values of the different bearings with different weight fractions but there is obvious reduction of the bending moment on the base of the piers in the case of using bearings comparing to the case of not using bearings in the connection between the superstructure and substructure.

6.2 **Further work**

Other effective mechanical properties of CNT/polymer composite like the interfacial shear strength can be changed to examine their effectiveness for the bridge seismic isolation.

More hazard events like (wind gust, flood, vessel collision, accidents, and terrorist attacks) can be simulated to examine the effect of the same bearings with different weight fractions and monitoring the bridge health over the time against these events.

References

1. Dresselhaus, M.S., G. Dresselhaus, and P.C. Eklund, *Chapter 20 - Applications of Carbon Nanostructures*, in *Science of Fullerenes and Carbon Nanotubes*, M.S. Dresselhaus, G. Dresselhaus, and P.C. Eklund, Editors. 1996, Academic Press: San Diego. p. 870-917.
2. Popov, V.N., *Carbon nanotubes: properties and application.* Materials Science and Engineering: R: Reports, 2004. **43**(3): p. 61-102.
3. Demczyk, B.G., et al., *Direct mechanical measurement of the tensile strength and elastic modulus of multiwalled carbon nanotubes.* Materials Science and Engineering: A, 2002. **334**(1): p. 173-178.
4. Thostenson, E.T., Z. Ren, and T.-W. Chou, *Advances in the science and technology of carbon nanotubes and their composites: a review.* Composites Science and Technology, 2001. **61**(13): p. 1899-1912.
5. Thostenson, E.T. and T.-W. Chou, *Aligned multi-walled carbon nanotube-reinforced composites: processing and mechanical characterization.* Journal of Physics D: Applied Physics, 2002. **35**(16): p. L77-L80.
6. Wu, A.S. and T.-W. Chou, *Carbon nanotube fibers for advanced composites.* Materials Today, 2012. **15**(7): p. 302-310.
7. Li, Q., J. Liu, and S. Xu, *Progress in Research on Carbon Nanotubes Reinforced Cementitious Composites.* Advances in Materials Science and Engineering, 2015. **2015**: p. 307435.
8. DeValve, C. and R. Pitchumani, *Experimental investigation of the damping enhancement in fiber-reinforced composites with carbon nanotubes.* Carbon, 2013. **63**: p. 71-83.
9. Spanos, K.N., S.K. Georgantzinos, and N.K. Anifantis, *Mechanical properties of graphene nanocomposites: A multiscale finite element prediction.* Composite Structures, 2015. **132**: p. 536-544.
10. Gupta, A.K. and S.P. Harsha, *Analysis of mechanical properties of carbon nanotube reinforced polymer composites using multi-scale finite element modeling approach.* Composites Part B: Engineering, 2016. **95**: p. 172-178.
11. Chen, W.-H., H.-C. Cheng, and Y.-L. Liu, *Radial mechanical properties of single-walled carbon nanotubes using modified molecular structure mechanics.* Computational Materials Science, 2010. **47**(4): p. 985-993.
12. Chandraseker, K. and S. Mukherjee, *Atomistic-continuum and ab initio estimation of the elastic moduli of single-walled carbon nanotubes.* Computational Materials Science, 2007. **40**(1): p. 147-158.
13. Agrawal, P.M., et al., *Molecular dynamics (MD) simulations of the dependence of C–C bond lengths and bond angles on the tensile strain in single-wall carbon nanotubes (SWCNT).* Computational Materials Science, 2008. **41**(4): p. 450-456.
14. Savvas, D.N., V. Papadopoulos, and M. Papadrakakis, *The effect of interfacial shear strength on damping behavior of carbon nanotube reinforced composites.* International Journal of Solids and Structures, 2012. **49**(26): p. 3823-3837.
15. Li, C. and T.-W. Chou, *Modeling of elastic buckling of carbon nanotubes by molecular structural mechanics approach.* Mechanics of Materials, 2004. **36**(11): p. 1047-1055.
16. Thostenson, E.T., C. Li, and T.-W. Chou, *Nanocomposites in context.* Composites Science and Technology, 2005. **65**(3): p. 491-516.
17. Cornell, W.D., et al., *A second generation force field for the simulation of proteins, nucleic acids, and organic molecules.* Journal of the American Chemical Society, 1995. **117**(19): p. 5179-5197.

18. Pal, G. and S. Kumar, *Modeling of carbon nanotubes and carbon nanotube–polymer composites.* Progress in Aerospace Sciences, 2016. **80**: p. 33-58.
19. Miehe, C. and A. Koch, *Computational micro-to-macro transitions of discretized microstructures undergoing small strains.* Archive of Applied Mechanics, 2002. **72**(4): p. 300-317.
20. Zhou, X., et al., *Interfacial damping characteristics of carbon nanotube-based composites.* Composites Science and Technology, 2004. **64**(15): p. 2425-2437.
21. Rahmat, M. and P. Hubert, *Carbon nanotube–polymer interactions in nanocomposites: A review.* Composites Science and Technology, 2011. **72**(1): p. 72-84.
22. Ganesan, Y., et al., *Interface Toughness of Carbon Nanotube Reinforced Epoxy Composites.* ACS Applied Materials & Interfaces, 2011. **3**(2): p. 129-134.
23. Wernik, J.M., B.J. Cornwell-Mott, and S.A. Meguid, *Determination of the interfacial properties of carbon nanotube reinforced polymer composites using atomistic-based continuum model.* International Journal of Solids and Structures, 2012. **49**(13): p. 1852-1863.
24. Papadopoulos, V. and M. Tavlaki, *The impact of interfacial properties on the macroscopic performance of carbon nanotube composites. A FE2-based multiscale study.* Composite Structures, 2016. **136**: p. 582-592.
25. Wuite, J. and S. Adali, *Deflection and stress behaviour of nanocomposite reinforced beams using a multiscale analysis.* Composite Structures, 2005. **71**(3): p. 388-396.
26. Kim, S.-H., H.-S. Mha, and S.-W. Lee, *Effects of bearing damage upon seismic behaviors of a multi-span girder bridge.* Engineering Structures, 2006. **28**(7): p. 1071-1080.
27. Li, J., T. Peng, and Y. Xu, *Damage investigation of girder bridges under the Wenchuan earthquake and corresponding seismic design recommendations.* Earthquake Engineering and Engineering Vibration, 2008. **7**(4): p. 337-344.
28. Han, Q., et al., *Seismic damage of highway bridges during the 2008 Wenchuan earthquake.* Earthquake Engineering and Engineering Vibration, 2009. **8**(2): p. 263-273.